Medullary Reticular Neurons Mediate Neuropeptide Y-Induced Metabolic Inhibition and Mastication

Yoshiko Nakamura,[1] Yuchio Yanagawa,[2] Shaun F. Morrison,[3]
Kazuhiro Nakamura[1,4,5,*]

[1]Department of Integrative Physiology, Nagoya University Graduate School of Medicine, Nagoya 466-8550, Japan

[2]Department of Genetic and Behavioral Neuroscience, Gunma University Graduate School of Medicine, Maebashi 371-8511, Japan

[3]Department of Neurological Surgery, Oregon Health & Science University, Portland, OR 97239, USA

[4]PRESTO, Japan Science and Technology Agency, Kawaguchi, Saitama 332-0012, Japan

[5]Lead Contact

*Correspondence: kazu@med.nagoya-u.ac.jp or nkazuhir@gmail.com

Published in *Cell Metabolism* 25: 322–334, 2017
http://dx.doi.org/10.1016/j.cmet.2016.12.002

This manuscript is accompanied by Supplemental Information containing Figures S1–S7, Supplemental Experimental Procedures, and Movie S1.

SUMMARY

Hypothalamic neuropeptide Y (NPY) elicits hunger responses to increase the chances of surviving starvation: an inhibition of metabolism and an increase in feeding. Here we elucidate a key central circuit mechanism through which hypothalamic NPY signals drive these hunger responses. GABAergic neurons in the intermediate and parvicellular reticular nuclei (IRt/PCRt) of the medulla oblongata, which are activated by NPY-triggered neural signaling from the hypothalamus, potentially through the nucleus tractus solitarius, mediate the NPY-induced inhibition of metabolic thermogenesis in brown adipose tissue (BAT) via their innervation of BAT sympathetic premotor neurons. Intriguingly, the GABAergic IRt/PCRt neurons innervating the BAT sympathetic premotor region also innervate the masticatory motor region, and stimulation of the IRt/PCRt elicits mastication and increases feeding as well as inhibits BAT thermogenesis. These results indicate that GABAergic IRt/PCRt neurons mediate hypothalamus-derived hunger signaling by coordinating both autonomic and feeding motor systems to reduce energy expenditure and to promote feeding.

Graphical abstract

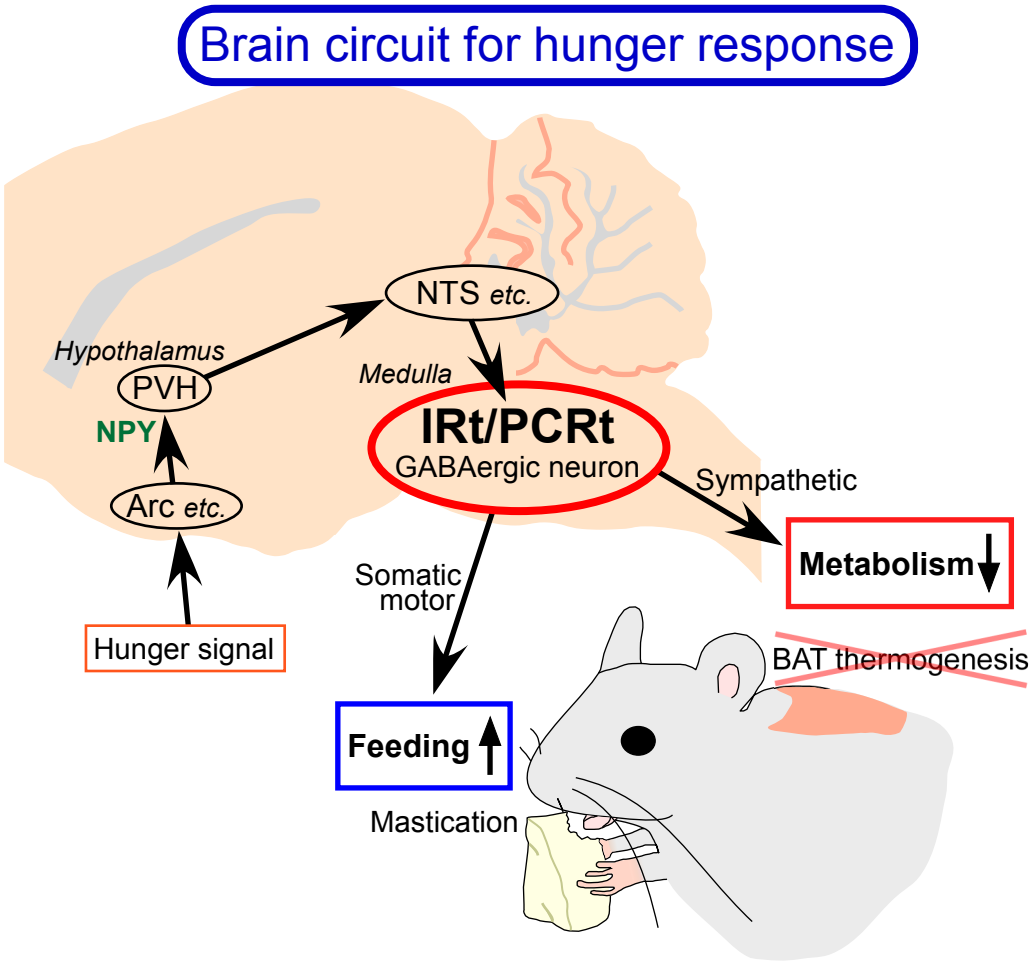

HIGHLIGHTS

• GABAergic IRt/PCRt neurons innervate sympathetic premotor neurons controlling BAT

• Selective activation of GABAergic IRt/PCRt neurons inhibits BAT thermogenesis

• Hypothalamic NPY inhibits BAT thermogenesis by activating GABAergic IRt/PCRt neurons

• GABAergic IRt/PCRt neurons can also mediate hunger-driven mastication and feeding

eTOC Blurb

Neuropeptide Y (NPY) released during negative energy balance triggers unknown hypothalamo-medullary neural signaling to elicit hunger responses: inhibition of metabolism and stimulation of feeding. Using *in vivo* physiology, chemogenetics and neuroanatomy, Nakamura et al. identified inhibitory medullary reticular neurons that mediate hypothalamic NPY-driven signaling to inhibit brown adipose tissue thermogenesis and stimulate mastication and feeding.

INTRODUCTION

Hunger stimulates appetite and reduces energy expenditure—innate physiological responses to improve energy balance between feeding bouts and to increase the chances of survival under more extreme starvation conditions. These hunger responses are driven by hypothalamic neural circuits, in which neuropeptide Y (NPY) plays a key role (Loh et al., 2015). NPY/agouti-related peptide (AgRP)-containing neurons in the arcuate nucleus of the hypothalamus are activated by peripheral hunger signaling mediated by hormones such as ghrelin secreted by the stomach (Kohno et al., 2003; Chen et al., 2015), and they release NPY from their axonal projections to other hypothalamic sites including the paraventricular hypothalamic nucleus (PVH) (Kalra et al., 1991). The hypothalamic action of NPY elicits an increase in food intake as well as a reduction in metabolism (Stanley and Leibowitz, 1985; Walker and Romsos, 1993; Atasoy et al., 2012). However, the central circuit mechanism by which the NPY-mediated hunger signaling from the hypothalamus coordinates the autonomic and somatic motor systems to reduce energy expenditure and to drive the consummatory responses remains unknown.

Hypothalamic release of NPY, including into the PVH, suppresses energy expenditure in excess of the basal metabolic rate by inhibiting active heat production, such as that occurring in brown adipose tissue (BAT) when animals, including humans (Betz and Enerbäck, 2015), are in a sub-thermoneutral environment (Egawa et al., 1991; Székely et al., 2005). BAT thermogenesis is an adaptive response to maintain body temperature in cold environments and to develop fever during infection, driven by the central sympathetic neural pathway descending from the thermoregulatory center in the preoptic area (Nakamura 2011; Morrison et al., 2014). In this pathway, BAT sympathetic premotor neurons in the

rostral medullary raphe region (rMR), including the rostral raphe pallidus and raphe magnus nuclei, play a key role by integrating information from various brain regions to provide excitatory commands to the spinal output system to drive BAT thermogenesis (Nakamura et al., 2004). These premotor neurons express vesicular glutamate transporter 3 (VGLUT3) and are activated by cold exposure or central administration of prostaglandin E_2 (PGE_2), a pyrogenic mediator (Nakamura et al., 2004). The important role of the sympathetic premotor neurons in the control of BAT thermogenesis and energy expenditure led us to hypothesize that NPY-mediated hunger signaling from the hypothalamus inhibits the premotor neurons to reduce the thermogenic sympathetic outflow to BAT.

In the present study, we sought to elucidate the central circuit mechanism by which the hypothalamic NPY-mediated hunger signal acts on the medullary motor systems to inhibit BAT thermogenesis and to stimulate feeding in a coordinated manner. To this end, we first sought to identify the neurons that mediate NPY-triggered signaling from the hypothalamus to inhibit BAT sympathetic premotor neurons, by using *in vivo* electrophysiological, neuroanatomical and chemogenetic techniques. Furthermore, we examined the possibility that the identified neurons are also involved in the NPY-stimulated feeding occurring synchronously with the inhibition of BAT thermogenesis.

RESULTS

NPY-Triggered Signaling from the PVH Inhibits BAT Thermogenesis through GABAergic Inputs to Sympathetic Premotor Neurons

To test the hypothesis that NPY-mediated hunger signaling from the hypothalamus inhibits BAT thermogenesis through inhibition of the sympathetic premotor outflow from the rMR, we examined the effect of

an injection of NPY into the rat hypothalamus on BAT thermogenesis evoked by stimulating sympathetic premotor neurons in the rMR. Consistent with the view that the sympathetic premotor drive for BAT thermogenesis is determined by the balance between excitatory (glutamatergic) and inhibitory (GABAergic) inputs to the premotor neurons (Nakamura 2011) (Figure 1A), either stimulation of NMDA glutamate receptors or blockade of $GABA_A$ receptors in the rMR elicited increases in BAT sympathetic nerve activity (SNA), BAT temperature, expired CO_2, heart rate and mean arterial pressure (Figure 1 and Figure S1). Nanoinjection of NPY into the PVH eliminated all the thermogenic and cardiovascular responses to the glutamatergic excitation of premotor neurons in the rMR with NMDA, but had no inhibitory effect on those evoked by blocking $GABA_A$ receptors in the rMR with bicuculline (Figure 1 and Figure S1). These results indicate that an action of NPY on PVH neurons leads to an inhibition of BAT thermogenesis and cardiovascular tone through a GABAergic inhibition of sympathetic premotor neurons in the rMR.

Medullary GABAergic Neurons Innervating BAT Sympathetic Premotor Neurons

To identify the source of the GABAergic inputs to the rMR through which NPY-mediated signaling from the PVH inhibits BAT sympathetic premotor neurons, we performed neural tract tracing studies. Cholera toxin b-subunit (CTb), a retrograde tracer, was injected into the rMR of *Gad1* (GAD67)-*Gfp* knock-in mice (Figure 2A), in which GABAergic neurons were labeled with GFP (Tamamaki et al., 2003). CTb labeling was found in many GFP-positive neurons in the intermediate reticular nucleus (IRt) and the parvicellular reticular nucleus (PCRt) of the medulla oblongata at the rostrocaudal levels around the rostral pole of the

inferior olivary complex (Figure 2B and C). Cell counting at three rostrocaudal levels (Figure 2C) showed that 42 ± 2% (n = 3 mice) of CTb-labeled IRt/PCRt neurons (45 ± 9 of 108 ± 16 cells) expressed GFP. Although a few double-positive neurons were also distributed in regions surrounding the IRt/PCRt (Figure 2C), such as the rostral ventrolateral medulla (RVL) (4 ± 1 GFP-positive in 30 ± 7 CTb-labeled cells) and the nucleus tractus solitarius (NTS) (6 ± 1 GFP-positive in 19 ± 2 CTb-labeled cells), no other medullary regions contained a substantial number of double-positive neurons.

Anterograde tracing from the IRt/PCRt with *Phaseolus vulgaris* leucoagglutinin (PHA-L) in rats (Figure 2D) labeled axon fibers and swellings in the rMR that contained vesicular GABA transporter (VGAT), a marker for GABAergic neurons, and that were closely associated with neuronal cell bodies and dendrites of VGLUT3-immunoreactive sympathetic premotor neurons (Figure 2E). Such putative synaptic connections of IRt/PCRt-derived GABAergic axons with VGLUT3-immunoreactive neurons were frequently found around a midline portion of the rMR (approximately 2–10 obvious appositions found by a brief confocal scanning of a 400 μm × 400 μm area). Because this microscopy likely missed many contacts of PHA-L-labeled fibers with the scarcely immunoreactive dendrites of VGLUT3-expressing neurons, more IRt/PCRt-derived GABAergic axons probably connect with those sympathetic premotor neurons. These retrograde and anterograde tracing results strongly support a direct innervation of BAT sympathetic premotor neurons in the rMR by GABAergic neurons in the IRt/PCRt.

Stimulation of GABAergic Neurons in the IRt/PCRt Inhibits BAT Thermogenic and Cardiac Responses

To investigate the role of neurons in the IRt/PCRt in the regulation of BAT thermogenesis, we examined the effect of stimulation of IRt/PCRt neurons on febrile BAT thermogenesis. Nanoinjection of PGE_2 into the rat preoptic area elicited intense BAT thermogenesis as well as metabolic (expired CO_2) and cardiovascular stimulation (Figure 3) (Nakamura et al., 2005). The PGE_2-evoked increases in BAT thermogenesis, metabolism and heart rate were reversed by unilateral stimulation of IRt/PCRt neurons with a nanoinjection of bicuculline, but not with saline (Figure 3A–D). There was no significant change in arterial pressure due to stimulation of IRt/PCRt neurons (Figure 3C), although it did increase in some cases (Figure 3A; Marchenko and Sapru, 2003). Mapping with bicuculline nanoinjections (Figure 3E) revealed the narrow distribution of the relevant IRt/PCRt neurons (2.6–2.8 mm caudal to the interaural line), since a rostral or caudal shift of only 0.3–0.5 mm in the position of the nanoinjections in the IRt/PCRt resulted in a drastically reduced inhibitory effect on the evoked BAT SNA.

Similar to NPY injection into the PVH (Figure 1D), stimulation of IRt/PCRt neurons failed to inhibit the BAT thermogenic, metabolic and tachycardic responses evoked by antagonizing $GABA_A$ receptors in the rMR with bicuculline (Figure S2). In contrast, stimulation of nearby RVL neurons did inhibit the rMR bicuculline-evoked responses (Figure S2; Cao et al., 2010) as well as the PGE_2-evoked BAT SNA (Figure 3E), indicating that IRt/PCRt neurons and RVL neurons are involved in distinct BAT sympathoinhibitory circuit mechanisms.

To directly examine whether activation of the GABAergic neurons in the IRt/PCRt inhibits BAT thermogenic and cardiac responses, we selectively stimulated GABAergic neurons in the IRt/PCRt *in vivo* by using a chemogenetic technique with hM3Dq, a G_q-coupled designer receptor exclusively activated by designer drug (DREADD; Roth 2016),

and examined the effects on BAT thermogenic and cardiac responses to cooling in mice. To achieve GABAergic neuron-specific expression of hM3Dq in the IRt/PCRt, adeno-associated virus (AAV) expressing the Cre-dependent *hM3Dq-mCherry* transgene (AAV-EF1α-DIO-hM3Dq-mCherry) was injected into the IRt/PCRt of *Gad2-IRES-Cre* knock-in mice, in which Cre recombinase was targeted to the *Gad2* (GAD65) gene (Taniguchi et al., 2011). Confirming the high selectivity of the expression of hM3Dq-mCherry in GABAergic neurons, injection of the AAV into the IRt/PCRt of *Gad2-IRES-Cre* knock-in mice crossed with the *Gad1-Gfp* knock-in strain resulted in 90% of hM3Dq-mCherry-expressing cells in the IRt/PCRt being GFP-positive, GABAergic neurons (Figure 4A; 169 GFP-positive in 188 hM3Dq-mCherry-expressing cells counted in 3 sections). Repeated skin cooling challenges to *Gad2-IRES-Cre* knock-in mice in which the AAV was bilaterally injected into the IRt/PCRt (Figure 4B) consistently increased BAT temperature and heart rate (Figure 4C). However, the cooling-induced BAT thermogenesis and tachycardia were eliminated following bilateral nanoinjections of the hM3Dq agonist, clozapine-*N*-oxide (CNO), into the IRt/PCRt to stimulate local GABAergic neurons, but not following vehicle injections into the IRt/PCRt (Figure 4C–E). Subsequent to the CNO treatment, inhibition of IRt/PCRt neurons with bilateral nanoinjections of muscimol, a $GABA_A$ receptor agonist widely used *in vivo* as a neuronal inhibitor, recovered the cooling-induced BAT thermogenesis and tachycardia (Figure 4C–E). Together with our tracing studies showing the IRt/PCRt–rMR GABAergic projection, these physiological results indicate that GABAergic neurons in the IRt/PCRt can inhibit BAT thermogenic and cardiac responses through their projections to sympathetic premotor neurons in the rMR.

Central NPY Activates GABAergic IRt/PCRt Neurons Projecting to the rMR

Whether GABAergic IRt/PCRt neurons projecting to the rMR are involved in central NPY-triggered neural circuit mechanisms was examined by performing *in vivo* unit recording in rats. Using collision tests (Figure 5A), we identified 11 IRt/PCRt neurons that were antidromically activated by electrical stimulation in the rMR. Ten of these IRt/PCRt neurons projecting to the rMR increased their firing rates in response to injection of NPY into the lateral ventricle (Figure 5B; before NPY, 5.3 ± 2.8 spikes/4 s; after NPY, 23.1 ± 6.4 spikes/4 s; $P < 0.01$, two-tailed paired *t*-test), while the other antidromically activated neuron showed no change in firing rate following NPY injection (before NPY, 0.14 spikes/4 s; after NPY, 0 spikes/4 s). The NPY-induced increases in neuronal firing rate were accompanied by decreases in BAT SNA (Figure 5B; before NPY, 744.3 ± 123.7% baseline; after NPY, 29.5 ± 7.6% baseline; $P < 0.001$). The average antidromic latency and estimated conduction velocity of these NPY-activated neurons were 12.5 ± 0.9 ms and 0.22 ± 0.02 m/s, respectively. Two of these neurons exhibited obvious phasic bursting patterns after NPY injection (Figure 5C).

Juxtacellular labeling following the unit recording was successful in 7 of the 11 antidromically activated IRt/PCRt neurons and confirmed their location in the IRt/PCRt (Figure 5D and E). To determine whether these labeled neurons were GABAergic, we performed *in situ* hybridization for mRNA of *Gad1* (GAD67), a marker for GABAergic neurons. Six of the juxtacellularly labeled neurons expressed *Gad1* and each of these was activated following the NPY injection, whereas the *Gad1*-negative neuron was the neuron unresponsive to NPY injection (Figure 5D and E). These results indicate that NPY-triggered neural

signaling activates GABAergic IRt/PCRt neurons projecting to the rMR, supporting the idea that this inhibitory transmission mediates the NPY-induced inhibition of BAT thermogenesis and tachycardia.

Inactivation of IRt/PCRt Neurons Eliminates NPY-Induced Inhibition of BAT Thermogenesis and Tachycardia

To further examine the involvement of IRt/PCRt neurons in the hypothalamic NPY-induced sympathoinhibition, we tested the effect of inactivation of IRt/PCRt neurons on the hypothalamic NPY-induced inhibition of BAT thermogenic and tachycardic responses to skin cooling. Cooling the rat trunk skin consistently evoked BAT thermogenic, metabolic and tachycardic responses (Nakamura and Morrison, 2007). These responses were all suppressed by a unilateral injection of NPY, but not saline, into either the PVH or the lateral ventricle (Figures 6, S3 and S4). Importantly, this inhibitory effect of NPY was reversed by inactivation of IRt/PCRt neurons with bilateral nanoinjections of muscimol, but not by saline injections (Figures 6 and S4). These results are consistent with the view that the inhibitory transmission from GABAergic IRt/PCRt neurons to sympathetic premotor neurons in the rMR mediates NPY-triggered signaling from the hypothalamus to inhibit the central sympathetic drives for adaptive BAT thermogenesis and metabolism and for tachycardia. The GABAergic innervation of the rMR by IRt/PCRt neurons does not provide a tonic basal sympathoinhibition, because muscimol injections into the IRt/PCRt by themselves did not elicit BAT thermogenesis (Figure 6B).

Stimulation of IRt/PCRt Neurons Evokes Mastication as well as Inhibits BAT Thermogenesis

Intriguingly, unilateral stimulation of IRt/PCRt neurons with a nanoinjection of bicuculline in anesthetized rats, which immediately reversed cooling-elevated BAT thermogenesis and heart rate, also evoked rhythmic masticatory movements of the masseter muscle with a frequency comparable to that observed following a central injection of NPY (Ushimura et al., 2015) (Figures 7A–C and S5, and Movie S1). The bicuculline injection also increased salivation in some animals. In free-moving rats, unilateral bicuculline injection into the IRt/PCRt promoted feeding behaviors with increased time spent chewing chow and bedding as well as increased food intake (Figure 7D and E), mimicking the feeding responses evoked by NPY injected into the PVH (Stanley and Leibowitz, 1985).

Thus, we examined the possibility that the GABAergic IRt/PCRt neurons projecting to the rMR are also involved in mastication. *Slc32a1* (VGAT)-*Venus* transgenic rats, in which GABAergic neurons are labeled with Venus (Uematsu et al., 2008) (Figure S6), received injections with the retrograde tracers, FluoroGold and CTb, into the rMR and the motor trigeminal nucleus (Mo5), respectively (Figure 7F), the latter containing masticatory motoneurons (Mizuno et al., 1975). Many neurons double-labeled with FluoroGold and CTb were distributed in the IRt/PCRt at 2.6–2.8 mm caudal to the interaural line (Figure 7G and H), coincident with the region in which neural stimulation strongly inhibited BAT thermogenesis (Figure 3E). Importantly, 73% of these double-labeled neurons (151 of 206 cells) in the IRt/PCRt expressed Venus (Figure 7G and H). This observation supports the view that the axons of GABAergic IRt/PCRt neurons bifurcate to masticatory motoneurons and to BAT sympathetic premotor neurons, thereby providing the circuit mechanism for NPY-mediated hunger signaling from the hypothalamus

to coordinate the promotion of mastication and feeding and the inhibition of adaptive thermogenesis (Figure 7I).

GABAergic IRt/PCRt Neurons Projecting to the rMR Receive Putative Synaptic Connections from the NTS and LPB

The PVH provides massive projections to the NTS, but much fewer to the IRt/PCRt (Shammah-Lagnado et al., 1992; Geerling et al., 2010; unpublished observation by Y.N. and K.N.). This observation raises the possibility that the BAT sympathoinhibitory, GABAergic IRt/PCRt neurons receive NPY-triggered signals from the hypothalamus by way of the NTS. Supporting this possibility, anterograde tracing with PHA-L injected into the NTS and retrograde tracing with FluoroGold injected into the rMR in *Slc32a1-Venus* transgenic rats showed close association of NTS-derived axon swellings with cell bodies of GABAergic IRt/PCRt neurons projecting to the rMR (Figure S7A and B).

The IRt/PCRt also receives projections, albeit fewer, from the lateral parabrachial nucleus (LPB) (Shammah-Lagnado et al., 1992), which has been proposed to receive a hunger signal from the PVH (Garfield et al., 2015). Injections of PHA-L and FluoroGold into the LPB and rMR, respectively, in *Slc32a1-Venus* transgenic rats visualized LPB-derived axon swellings apposed to cell bodies of GABAergic IRt/PCRt neurons projecting to the rMR (Figure S7C and D). However, PHA-L-labeled fibers from the LPB were more sparsely distributed in the IRt/PCRt than those from the NTS. These anatomical observations indicate that GABAergic IRt/PCRt neurons innervating the rMR can receive inputs from the NTS and LPB (Figure 7I).

DISCUSSION

Reduced energy expenditure and stimulated appetite are fundamental innate strategies that mammals use to survive starvation, and may, perhaps to a lesser extent, be employed in normal feeding cycles. Many studies have focused on the hypothalamic circuit that provides command signals to elicit the physiological and behavioral responses upon receiving hunger signals from peripheral organs, such as ghrelin (Loh et al., 2015). In this circuit, NPY is well known as a powerful hypothalamic neuropeptide that can trigger the hunger responses (Loh et al., 2015). However, the circuit mechanism by which the commands from the hypothalamic network affect the medullary motor systems to alter autonomic thermogenesis and feeding motor functions has been poorly understood. The present study highlights the IRt/PCRt as an important component in the hypothalamomedullary hunger response circuit. We showed that GABAergic neurons in the IRt/PCRt provide direct axonal projections to the rMR with putative synaptic connections to BAT sympathetic premotor neurons, and that activation of neurons in the limited area of the IRt/PCRt eliminates BAT thermogenesis and tachycardia evoked by skin cooling or pyrogenic stimulation. Furthermore, our chemogenetic experiments demonstrated that a GABAergic population of IRt/PCRt neurons is responsible for the sympathoinhibitory effects. These findings indicate that GABAergic IRt/PCRt neurons can suppress BAT thermogenesis and tachycardia through their inhibitory inputs to sympathetic premotor neurons in the rMR.

In support of this view, stimulation of IRt/PCRt neurons failed to inhibit BAT thermogenesis and tachycardia evoked by disinhibition of sympathetic premotor neurons effected by antagonizing $GABA_A$ receptors in the rMR. Similarly, NPY injection into the PVH, which

inhibited BAT thermogenesis and cardiovascular responses to glutamatergic stimulation of sympathetic premotor neurons in the rMR, failed to inhibit the thermogenic and cardiovascular responses evoked by antagonizing $GABA_A$ receptors in the rMR. These results indicate that hypothalamic NPY-triggered neural signaling also inhibits BAT thermogenesis and tachycardia through GABAergic inhibition of sympathetic premotor neurons in the rMR. Consistently, the present *in vivo* unit recording followed by *in situ* hybridization showed that NPY-triggered neural signaling activates GABAergic transmission from the IRt/PCRt to the rMR. Furthermore, inactivation of IRt/PCRt neurons blocked the inhibitory effects of hypothalamic NPY on BAT thermogenesis and tachycardia. All these results support the view that NPY-mediated neural signaling from the hypothalamus in response to negative energy balance activates GABAergic transmission from the IRt/PCRt to sympathetic premotor neurons in the rMR to suppress the excitatory outflows driving active BAT thermogenesis and tachycardia for cold defense and the development of fever (Figure 7I). This mechanism is consistent with the physiological action of central NPY that inhibits active heat production in sub-thermoneutral environments, but not basal metabolic rate (Székely et al., 2005).

The present study revealed that many GABAergic IRt/PCRt neurons innervating the BAT sympathetic premotor region (rMR) also innervate the masticatory motor region (Mo5). Indicating the involvement of IRt/PCRt neurons in the control of both mastication and metabolism, stimulation of IRt/PCRt neurons elicited mastication as well as an inhibition of BAT thermogenesis. Surprisingly, stimulation of IRt/PCRt neurons in free-moving rats increased chewing and feeding, similar to the action of hypothalamic NPY (Stanley and Leibowitz, 1985; Ushimura et al., 2015). Supporting the critical function of the IRt/PCRt in the

orexigenic action of NPY, inactivation of IRt/PCRt neurons reduces mastication and feeding elicited by hypothalamic NPY (Travers et al., 2010). The IRt/PCRt contains masticatory premotor neurons, some of which are GABAergic (Li et al., 1996; Travers et al., 2005), and constitutes the central pattern generator for the rhythmic masticatory muscle movements (Moore et al., 2014). Although the circuit mechanism of the central pattern generator has yet to be determined, both glutamatergic and GABAergic premotor inputs from the IRt/PCRt to the Mo5 are likely activated for the generation of the rhythmic masticatory motor activities (Nakamura and Katakura, 1995) including the NPY-induced mastication. Phasic bursting patterns similar to masticatory rhythm were observed in our unit recording from GABAergic, rMR-projecting IRt/PCRt neurons (Figure 5C), suggesting the involvement of these IRt/PCRt neurons in the NPY-induced mastication (Figure 7I).

The NPY-triggered masticatory premotor signaling from the IRt/PCRt likely primes the motor system to be "ready to eat", and the final motor output may be gated by corticomedullary inputs (Nakamura and Katakura, 1995; Moore et al., 2014), which could be triggered by visual and olfactory sensation of food, to initiate mastication dependent on food availability. Under the anesthetized condition in the present study, the mastication we observed following stimulation of IRt/PCRt neurons was likely due to an anesthesia-mediated reduction of such a top-down control of mastication from the cerebral cortex. On the other hand, our selective chemogenetic stimulation of GABAergic neurons in the IRt/PCRt did not elicit masticatory movements (unpublished observation by Y.N. and K.N.), probably because the masticatory motor rhythm generation requires activation of both GABAergic and glutamatergic premotor neurons in the IRt/PCRt. The paucity of non-GABAergic IRt/PCRt neurons projecting to both the rMR and Mo5 (Figure 7H)

suggests that GABAergic masticatory premotor neurons in the IRt/PCRt, rather than glutamatergic ones, mediate the NPY-triggered inhibition of BAT thermogenesis through their axon collaterals to the rMR (Figure 7I).

Although it is still uncertain how the NPY-mediated signal is transmitted from the PVH to the IRt/PCRt, the PVH provides massive projections to the NTS (Geerling et al., 2010), and our tracing study revealed putative synaptic connections of axons from the NTS to GABAergic IRt/PCRt neurons innervating the rMR (Figure S7). Furthermore, stimulation of rostral NTS neurons inhibited BAT thermogenesis (Figure 3E). The insignificant number of GABAergic neurons in the rostral NTS that project to the rMR in either mice or rats (Figures 2C and 7H) indicates negligible monosynaptic inhibitory innervation from the NTS to the rMR. Therefore, NTS neurons could mediate the NPY-triggered signaling from the hypothalamus to GABAergic IRt/PCRt neurons to indirectly inhibit sympathetic premotor neurons in the rMR. Because the NTS receives a variety of vagal visceral afferents, some of which may inhibit BAT SNA (Morrison et al, 2014; Madden et al, 2016), the hypothalamic NPY signal could be integrated with nutritional visceral information impinging on NTS neurons before being transmitted to the IRt/PCRt (Figure 7I).

We also found that GABAergic IRt/PCRt neurons innervating the rMR receive putative synaptic inputs from the LPB. The LPB, but not the NTS, receives excitatory inputs from melanocortin-4 receptor (MC4R)-expressing neurons in the PVH and optogenetic stimulation of this transmission to the LPB alters food intake (Garfield et al., 2015). NPY/AgRP/GABA-containing axons from the arcuate nucleus provide synaptic inputs to 83% of MC4R-expressing neurons and 20% of non-MC4R neurons in the PVH (Garfield et al., 2015). Although the present study only examined the NPY-triggered hunger response signaling, AgRP,

co-released from arcuate NPY neurons, can decrease metabolism and increase feeding by inhibiting the melanocortin system through antagonizing MC4Rs in the PVH (Cowley et al., 1999; Sohn et al., 2013). The responses induced by AgRP are likely mediated by neural pathways different from those mediating the NPY-triggered hunger responses (Krashes et al., 2013). Together with our present finding, therefore, AgRP released in the PVH may trigger a hunger response signaling through the PVH–LPB–IRt/PCRt pathway by antagonizing melanocortin inputs to MC4R-expressing PVH neurons. In this hypothesis, whether GABAergic IRt/PCRt neurons mediate the AgRP-triggered signaling is an attractive question awaiting further investigation. On the other hand, NPY might act on non-MC4R PVH neurons, potentially oxytocin neurons (Atasoy et al., 2012), to stimulate hunger response signaling through the PVH–NTS–IRt/PCRt pathway. It should be noted that NPY receptor-expressing PVH neurons can receive NPY through its volume transmission even if they do not all receive NPY/AgRP neuron synaptic inputs.

Whether NPY activates or inhibits PVH neurons is controversial (Mercer et al., 2011). NPY activates (disinhibits) PVH neurons by inhibiting GABA release from terminals that synapse on parvocellular PVH neurons (Cowley et al., 1999; Pronchuk et al., 2002), and central NPY injection induces expression of Fos, a marker of neuronal activation, in PVH neurons (Li et al., 1994). Similar to NPY injection into the PVH, non-selective stimulation of PVH neurons with NMDA or bicuculline inhibits BAT thermogenesis evoked by glutamatergic stimulation of the rMR, but not that evoked by antagonizing $GABA_A$ receptors in the rMR (Madden and Morrison, 2009). This similarity of the effects of NPY and the non-selective neural stimulation in the PVH supports the view that activation of PVH neurons by NPY gives rise to

the descending signal that activates the IRt/PCRt–rMR GABAergic transmission to inhibit BAT thermogenesis. On the other hand, NPY also postsynaptically inhibits the discharge of MC4R-expressing PVH neurons (Ghamari-Langroudi et al., 2011). Optogenetic stimulation of NPY/AgRP/GABA neuronal transmission from the arcuate nucleus to the PVH evokes inhibitory postsynaptic currents in PVH neurons and also elicits a hyperphagic response that is reduced by antagonizing either NPY or $GABA_A$ receptors in the PVH (Atasoy et al., 2012). If inhibition of PVH neurons by NPY leads to the stimulation of the IRt/PCRt–rMR GABAergic transmission, the pathway from the PVH to the IRt/PCRt would involve a disinhibitory mechanism, which awaits further investigation.

NPY-containing neurons are also distributed in the dorsomedial hypothalamus (DMH) in addition to the arcuate nucleus and knockdown of NPY expression in the DMH increases energy expenditure and thermogenic responses to cold (Chao et al., 2011), suggesting a role of DMH-derived NPY in reducing metabolism and BAT thermogenesis. The projections of NPY-containing DMH neurons are mostly limited to hypothalamic regions including the PVH (Lee et al., 2013). In the present study, NPY injection into the lateral ventricle, as well as into the PVH, strongly inhibited skin cooling-evoked BAT thermogenesis and tachycardia, and, independent of injection site, the inhibitory effects of NPY were completely reversed by inactivation of IRt/PCRt neurons. This result indicates that IRt/PCRt neurons mediate NPY-triggered sympathoinhibitory signaling not only from the PVH, but also from any other hypothalamic sites at which NPY may act.

The IRt/PCRt has never been associated with the control of thermogenesis or metabolism. The present study demonstrates that GABAergic neurons in this medullary reticular formation function in the

hypothalamomedullary hunger response signaling to inhibit sympathetic premotor outflows to BAT and the heart to reduce energy expenditure for the survival of starvation. Our results also show that these GABAergic neurons can contribute to the generation of masticatory premotor activities to enable the animals to initiate food intake as soon as it becomes available. These findings clearly indicate that the IRt/PCRt coordinates the autonomic and somatic motor systems in response to the hunger signaling from the hypothalamus to drive the metabolic and consummatory hunger responses (Figure 7I). Hyperactivity of the GABAergic IRt/PCRt neurons under non-starved conditions likely contributes to the development of pathological states leading to obesity. The inputs and the mechanisms that regulate the activity of GABAergic IRt/PCRt neurons will be a next focus of interest.

EXPERIMENTAL PROCEDURES

Animals

Male Sprague-Dawley (SD) rats (200–500 g), male *Slc32a1-Venus* (VGAT-Venus-B) transgenic rats (also known as *Tg(Slc32a1-YFP*)2Yyan*; 250–500 g; Uematsu et al., 2008), male *Gad1-Gfp* (GAD67-GFP) knock-in mice (also known as $Gad1^{tm1.1Tama}$; 25–40 g; Tamamaki et al., 2003) and male *Gad2-IRES-Cre* (GAD65-ires-Cre) knock-in mice (also known as $Gad2^{tm2(cre)Zjh}$; 25–30 g; Jackson Laboratory stock 010802; Taniguchi et al., 2011) were used. They were housed two or three to a cage with *ad libitum* access to food and water in a room air-conditioned at 24 ± 2˚C with a standard 12 h light/dark cycle before used for surgery or experiments. All procedures conform to the guidelines of animal care by the Division of Experimental Animals, Nagoya University Graduate School of Medicine and to the regulations detailed in the National Institutes of Health Guide for the Care and Use of Laboratory

Animals, and were approved by the Nagoya University Animal Experiment Committee and by the Animal Care and Use Committee of the Oregon Health & Science University.

Neural tract tracing

Animals received injections of Alexa594-conjugated CTb (Invitrogen), FluoroGold (Fluorochrome) or PHA-L (Vector) into a specific brain site under deep anesthesia (see Supplemental Experimental Procedures). Four to eight days after the tracer injection, the animals were re-anesthetized and transcardially perfused with saline and then with 4% (or 2% for VGLUT3 immunohistochemistry) formaldehyde in 0.1 M phosphate buffer (pH 7.4). The brain was removed, postfixed in the fixative at 4˚C for 2–3 hrs, and then cryoprotected in a 30% sucrose solution overnight. The tissue was cut into 30-μm-thick (rat) or 20-μm-thick (mouse) frontal sections on a freezing microtome. Data from animals where tracer injection was not centered in the target brain region were excluded. CTb and PHA-L were detected in the brain sections with immunohistochemical staining and FluoroGold was detected with the fluorescence of the tracer.

Immunohistochemistry

Immunohistochemistry followed our methods (Nakamura et al., 2004, 2005; see Supplemental Experimental Procedures). The primary antibodies used are anti-CTb goat serum (#703, List Biological Laboratories), anti-GFP mouse antibody (A11120, Life Technologies), anti-GFP guinea pig serum (Tamamaki et al., 2000), anti-mRFP rabbit antibody (Hioki et al., 2010), anti-PHA-L rabbit antibody (AL-1801-2, EY laboratories), anti-PHA-L goat antibody (AS-2224, Vector), anti-VGLUT3 guinea pig antibody (Hioki et al., 2004), and anti-VGAT rabbit

antibody (VGAT11-A, Alpha Diagnostics). The anti-GFP mouse antibody and the anti-mRFP antibody showed reactivity to Venus and mCherry, respectively.

In situ hybridization

In situ hybridization for *Gad1* mRNA was performed according to our previous method (Nakamura et al., 2002), except the hybridization signals were visualized with Fast Red according to manufacturer's guide (Roche). For subsequent immunofluorescence labeling of Venus, the sections were incubated with an anti-heat-denatured GFP rabbit antibody (1 μg/ml; Nakamura et al., 2008). The immunoreactivity was visualized by incubating the sections with a biotinylated donkey antibody to rabbit IgG (1:100; AP182B, Millipore) and then with 2 μg/ml Alexa488-conjugated streptavidin (S11223, Invitrogen).

In vivo electrophysiology in anesthetized rats

The procedure for *in vivo* physiological recordings basically followed our previous studies (Nakamura and Morrison, 2007, 2011; see Supplemental Experimental Procedures). In SD rats anesthetized with urethane and α-chloralose, postganglionic BAT SNA was electrophysiologically recorded from a nerve bundle isolated from the right interscapular BAT pad. Temperature of the left interscapular BAT pad, rectal temperature, trunk skin temperature, mixed expired CO_2, arterial pressure, and heart rate were also recorded simultaneously. In some animals, electromyogram (EMG) was also recorded with bipolar needle electrodes inserted into the masseter muscle.

In vivo unit recording was performed as described (Nakamura and Morrison, 2008, 2010) with a recording glass microelectrode filled with 0.5 M sodium acetate (DC resistance: 18–39 MΩ) containing 5%

biotinamide to allow juxtacellular labeling of the recorded neurons. A monopolar tungsten stimulating microelectrode was stereotaxically positioned in the rMR. The IRt/PCRt was explored with the recording electrode for neurons showing a constant onset latency response to electrical stimulation in the rMR (0.2–3 mA, 1 ms, 0.25–0.33 Hz). Standard criteria (Morrison and Cao, 2000) were used to establish the antidromic nature of the responses of IRt/PCRt neurons to rMR stimulation. After time-controlled collision tests (Figure 5A), the effects of an NPY injection into the lateral ventricle (1 mg/ml, 5 μl) on the spontaneous firing rate of the antidromically identified neuron and on cooling-increased BAT SNA and BAT temperature were tested. For juxtacellular labeling (Pinault, 1996) of the recorded neurons with biotinamide, positive current pulses (0.5–4.0 nA, 200 ms duration, 50% duty cycle) were delivered for 1–5 min to entrain the neuron. After the recording, the animals were perfused with 4% formaldehyde and the labeled neurons were visualized by incubating the brain sections with 1 μg/ml Alexa488-conjugated streptavidin. The sections were further processed for *in situ* hybridization to detect *Gad1* mRNA expression as above. For firing rate analysis of each recorded neuron, the rate of spontaneous firing was measured as spikes/4 s and averaged for 30 s immediately before NPY injection and after NPY-induced inhibition of BAT SNA to compare.

In vivo chemogenetic experiment in anesthetized mice

Gad2-IRES-Cre knock-in mice received bilateral injections into the IRt/PCRt with AAV-EF1α-DIO-hM3Dq-mCherry. More than 1 week later, the mice were anesthetized with urethane, and their interscapular BAT temperature, abdominal skin temperature, rectal temperature and heart rate (converted from electrocardiogram) were monitored (see

Supplemental Experimental Procedures). CNO (0.1 mg/ml, dissolved in 0.5% DMSO), vehicle (0.5% DMSO in saline) or 2 mM muscimol was injected bilaterally into the IRt/PCRt (30 nl/site) and subsequently, the abdominal skin was cooled and rewarmed repetitively by using a water jacket. The effects of the injectates on skin cooling-induced BAT thermogenesis and tachycardia were tested in the order of vehicle, CNO and muscimol.

Bicuculline injection into the IRt/PCRt in free-moving rats

SD rats received a unilateral nanoinjection of 2 mM bicuculline or saline (50–100 nl) into the IRt/PCRt through a pre-implanted cannula. Food intake and chewing time were measured in feeding monitoring cages (Feedam, Melquest) for 1 hr after the injection. For detailed procedure, see Supplemental Experimental Procedures.

Anatomy and Statistical Analysis

We adopted the cytoarchitecture and nomenclature of most brain regions from those of Paxinos and Watson (1998) for rats and Franklin and Paxinos (2007) for mice. The raphe pallidus nucleus was nomenclaturally divided into two parts, rostral (rRPa) and caudal (cRPa), at the rostral end of the inferior olivary complex (Nakamura et al., 2002, 2004).

Data are shown as the means ± SEM. Statistic comparison analyses were performed using a paired or unpaired *t*-test, Mann-Whitney test, a repeated measures one-way ANOVA followed by Tukey's multiple comparisons test, or a two-way ANOVA followed by Bonferroni's multiple comparisons test (Prism 6, GraphPad) as stated in the text and figure legends. All the statistic tests were two-sided. $P < 0.05$ was considered statistically significant.

SUPPLEMENTAL INFORMATION

Supplemental Information includes 7 figures, Supplemental Experimental Procedures and 1 movie.

AUTHOR CONTRIBUTIONS

Y.N., S.F.M and K.N. designed and performed experiments. Y.N. and K.N. analyzed data. Y.Y. provided *Gad1-Gfp* knock-in mice and *Slc32a1-Venus* transgenic rats. Y.N., S.F.M and K.N. discussed data and wrote the manuscript, and all authors approved the manuscript.

ACKNOWLEDGMENTS

We thank Chika Tanizawa and Miki Iwatani for anatomical assistance, Naoya Kataoka for providing AAV, Hiroyuki Hioki for providing anti-VGLUT3, anti-GFP, anti-denatured GFP and anti-mRFP antibodies, and Atsushi Miyawaki for providing pCS2-Venus. This study was supported by the Funding Program for Next Generation World-Leading Researchers from the Japan Society for the Promotion of Science (LS070 to K.N.), by Grants-in-Aid for Scientific Research (16H05128, 15H05932, 15K21744, 26118508 and 26713009 to K.N., 26290002 and 15H01415 to Y.Y., and 26860159 to Y.N.) and a Grant-in-Aid for Scientific Research on Innovative Areas (Comprehensive Brain Science Network) (to Y.Y.) from the MEXT of Japan, by the U.S. NIH grant (R01NS40987 to S.F.M.), and by grants from the Takeda Science Foundation (to K.N. and Y.Y.), Nakajima Foundation, Uehara Memorial Foundation, Brain Science Foundation, and Kowa Life Science Foundation (to K.N.).

REFERENCES

Atasoy, D., Betley, J.N., Su, H.H., and Sternson, S.M. (2012). Deconstruction of a neural circuit for hunger. Nature *488*, 172–177.

Betz, M.J., and Enerbäck, S. (2015). Human brown adipose tissue: what we have learned so far. Diabetes *64*, 2352–2360.

Cao, W.H., Madden, C.J., and Morrison, S.F. (2010). Inhibition of brown adipose tissue thermogenesis by neurons in the ventrolateral medulla and in the nucleus tractus solitarius. Am. J. Physiol. Regul. Integr. Comp. Physiol. *299*, R277–R290.

Chao, P.T., Yang, L., Aja, S., Moran, T.H., and Bi, S. (2011). Knockdown of NPY expression in the dorsomedial hypothalamus promotes development of brown adipocytes and prevents diet-induced obesity. Cell Metab. *13*, 573–583.

Chen, Y., Lin, Y.C., Kuo, T.W., and Knight, Z.A. (2015). Sensory detection of food rapidly modulates arcuate feeding circuits. Cell *160*, 829–841.

Cowley, M.A., Pronchuk, N., Fan, W., Dinulescu, D.M., Colmers, W.F., and Cone, R.D. (1999). Integration of NPY, AGRP, and melanocortin signals in the hypothalamic paraventricular nucleus: evidence of a cellular basis for the adipostat. Neuron *24*, 155–163.

Egawa, M., Yoshimatsu, H., and Bray, G.A. (1991). Neuropeptide Y suppresses sympathetic activity to interscapular brown adipose tissue in rats. Am. J. Physiol. *260*, R328–R334.

Franklin, K.B.J., and Paxinos, G. (2007). The Mouse Brain in Stereotaxic Coordinates, Third Edition (London: Academic Press).

Garfield, A.S., Li, C., Madara, J.C., Shah, B.P., Webber, E., Steger, J.S., Campbell, J.N., Gavrilova, O., Lee, C.E., Olson, D.P., Elmquist, J.K., Tannous, B.A., Krashes, M.J., and Lowell, B.B. (2015). A neural basis

for melanocortin-4 receptor-regulated appetite. Nat. Neurosci. *18*, 863–871.

Geerling, J.C., Shin, J.W., Chimenti, P.C., and Loewy, A.D. (2010). Paraventricular hypothalamic nucleus: axonal projections to the brainstem. J. Comp. Neurol. *518*, 1460–1499.

Ghamari-Langroudi, M., Srisai, D., and Cone, R.D. (2011). Multinodal regulation of the arcuate/paraventricular nucleus circuit by leptin. Proc. Natl. Acad. Sci. U.S.A. *108*, 355–360.

Hioki, H., Fujiyama, F., Nakamura, K., Wu, S.X., Matsuda, W., and Kaneko, T. (2004). Chemically specific circuit composed of vesicular glutamate transporter 3- and preprotachykinin B-producing interneurons in the rat neocortex. Cereb. Cortex *14*, 1266–1275.

Hioki, H., Nakamura, H., Ma, Y.F., Konno, M., Hayakawa, T., Nakamura, K.C., Fujiyama, F., and Kaneko, T. (2010). Vesicular glutamate transporter 3-expressing nonserotonergic projection neurons constitute a subregion in the rat midbrain raphe nuclei. J. Comp. Neurol. *518*, 668–686.

Kalra, S.P., Dube, M.G., Sahu, A., Phelps, C.P., and Kalra, P.S. (1991). Neuropeptide Y secretion increases in the paraventricular nucleus in association with increased appetite for food. Proc. Natl. Acad. Sci. U.S.A. *88*, 10931–10935.

Kohno, D., Gao, H.Z., Muroya, S, Kikuyama, S., and Yada, T. (2003). Ghrelin directly interacts with neuropeptide-Y-containing neurons in the rat arcuate nucleus: Ca^{2+} signaling via protein kinase A and N-type channel-dependent mechanisms and cross-talk with leptin and orexin. Diabetes *52*, 948–956.

Krashes, M.J., Shah, B.P., Koda, S., and Lowell, B.B. (2013). Rapid versus delayed stimulation of feeding by the endogenously released

AgRP neuron mediators GABA, NPY, and AgRP. Cell Metab. *18*, 588–595.

Lee, S.J., Kirigiti, M., Lindsley, S.R., Loche, A., Madden, C.J., Morrison, S.F., Smith, M.S., and Grove, K.L. (2013). Efferent projections of neuropeptide Y-expressing neurons of the dorsomedial hypothalamus in chronic hyperphagic models. J. Comp. Neurol. *521*, 1891–1914.

Li, B.H., Xu, B., Rowland, N.E., and Kalra, S.P. (1994). c-*fos* expression in the rat brain following central administration of neuropeptide Y and effects of food consumption. Brain Res. *665*, 277–284.

Li, Y.Q., Takada, M., Kaneko, T., and Mizuno, N. (1996). GABAergic and glycinergic neurons projecting to the trigeminal motor nucleus: a double labeling study in the rat. J. Comp. Neurol. *373*, 498–510.

Loh, K., Herzog, H., and Shi, Y.C. (2015). Regulation of energy homeostasis by the NPY system. Trends Endocrinol. Metab. *26*, 125–135.

Madden, C.J., da Conceicao, E.P.S., and Morrison, S.F. (2016). Vagal afferent activation decreases brown adipose tissue (BAT) sympathetic nerve activity and BAT thermogenesis. Temperature http://dx.doi.org/10.1080/23328940.2016.1257407.

Madden, C.J., and Morrison, S.F. (2009). Neurons in the paraventricular nucleus of the hypothalamus inhibit sympathetic outflow to brown adipose tissue. Am. J. Physiol. Regul. Integr. Comp. Physiol. *296*, R831–R843.

Marchenko, V., and Sapru, H.N. (2003). Cardiovascular responses to chemical stimulation of the lateral tegmental field and adjacent medullary reticular formation in the rat. Brain Res. *977*, 247–260.

Mercer, R.E., Chee, M.J., and Colmers, W.F. (2011). The role of NPY in hypothalamic mediated food intake. Front Neuroendocrinol. *32*, 398–415.

Mizuno, N., Konishi, A., and Sato, M. (1975). Localization of masticatory motoneurons in the cat and rat by means of retrograde axonal transport of horseradish peroxidase. J. Comp. Neurol. *164*, 105–115.

Moore, J.D., Kleinfeld, D., and Wang, F. (2014). How the brainstem controls orofacial behaviors comprised of rhythmic actions. Trends Neurosci. *37*, 370–380.

Morrison, S.F. and Cao, W.H. (2000). Different adrenal sympathetic preganglionic neurons regulate epinephrine and norepinephrine secretion. Am. J. Physiol. Regul. Integr. Comp. Physiol. *279*, R1763–R1775.

Morrison, S.F., Madden, C.J., and Tupone, D. (2014). Central neural regulation of brown adipose tissue thermogenesis and energy expenditure. Cell Metab. *19*, 741–756.

Nakamura, K. (2011). Central circuitries for body temperature regulation and fever. Am. J. Physiol. Regul. Integr. Comp. Physiol. *301*, R1207–R1228.

Nakamura, K., Matsumura, K., Kaneko, T., Kobayashi, S., Katoh, H., and Negishi, M. (2002). The rostral raphe pallidus nucleus mediates pyrogenic transmission from the preoptic area. J. Neurosci. *22*, 4600–4610.

Nakamura, K., Matsumura, K., Hübschle, T., Nakamura, Y., Hioki, H., Fujiyama, F., Boldogköi, Z., König, M., Thiel, H.J., Gerstberger, R., et al. (2004). Identification of sympathetic premotor neurons in medullary raphe regions mediating fever and other thermoregulatory functions. J. Neurosci. *24*, 5370–5380.

Nakamura, K., and Morrison, S.F. (2007). Central efferent pathways mediating skin cooling-evoked sympathetic thermogenesis in brown

adipose tissue. Am. J. Physiol. Regul. Integr. Comp. Physiol. *292*, R127–R136.

Nakamura, K., and Morrison, S.F. (2008). A thermosensory pathway that controls body temperature. Nat. Neurosci. *11*, 62–71.

Nakamura, K., and Morrison, S.F. (2010). A thermosensory pathway mediating heat-defense responses. Proc. Natl. Acad. Sci. U.S.A. *107*, 8848–8853.

Nakamura, K., and Morrison, S.F. (2011). Central efferent pathways for cold-defensive and febrile shivering. J. Physiol. *589*, 3641–3658.

Nakamura, K.C., Kameda, H., Koshimizu, Y., Yanagawa, Y., and Kaneko, T. (2008). Production and histological application of affinity-purified antibodies to heat-denatured green fluorescent protein. J. Histochem. Cytochem. *56*, 647–657.

Nakamura, Y., and Katakura, N. (1995). Generation of masticatory rhythm in the brainstem. Neurosci. Res. *23*, 1–19.

Nakamura, Y., Nakamura, K., Matsumura, K., Kobayashi, S., Kaneko, T., and Morrison, S.F. (2005). Direct pyrogenic input from prostaglandin EP3 receptor-expressing preoptic neurons to the dorsomedial hypothalamus. Eur. J. Neurosci. *22*, 3137–3146.

Paxinos, G., and Watson, C. (1998). The Rat Brain in Stereotaxic Coordinates, Fourth Edition (London: Academic Press).

Pinault, D. (1996). A novel single-cell staining procedure performed in vivo under electrophysiological control: morpho-functional features of juxtacellularly labeled thalamic cells and other central neurons with biocytin or Neurobiotin. J. Neurosci. Methods. *65*, 113–136.

Pronchuk, N., Beck-Sickinger, A.G., and Colmers, W.F. (2002). Multiple NPY receptors Inhibit $GABA_A$ synaptic responses of rat medial parvocellular effector neurons in the hypothalamic paraventricular nucleus. Endocrinology *143*, 535–543.

Roth, B.L. (2016). DREADDs for neuroscientists. Neuron *89*, 683–694.

Shammah-Lagnado, S.J., Costa, M.S.M.O., and Ricardo, J.A. (1992). Afferent connections of the parvocellular reticular formation: a horseradish peroxidase study in the rat. Neuroscience *50*, 403–425.

Sohn, J.W., Elmquist, J.K., and Williams, K.W. (2013). Neuronal circuits that regulate feeding behavior and metabolism. Trends Neurosci. *36*, 504–512.

Stanley, B.G., and Leibowitz, S.F. (1985). Neuropeptide Y injected in the paraventricular hypothalamus: a powerful stimulant of feeding behavior. Proc. Natl. Acad. Sci. U.S.A. *82*, 3940–3943.

Székely, M., Pétervári, E., Pákai, E., Hummel, Z., and Szelényi, Z. (2005). Acute, subacute and chronic effects of central neuropeptide Y on energy balance in rats. Neuropeptides *39*, 103–115.

Tamamaki, N., Nakamura, K., Furuta, T., Asamoto, K., and Kaneko, T. (2000). Neurons in Golgi-stain-like images revealed by GFP-adenovirus infection in vivo. Neurosci. Res. *38*, 231–236.

Tamamaki, N., Yanagawa, Y., Tomioka, R., Miyazaki, J., Obata, K., and Kaneko, T. (2003). Green fluorescent protein expression and colocalization with calretinin, parvalbumin, and somatostatin in the GAD67-GFP knock-in mouse. J. Comp. Neurol. *467*, 60–79.

Taniguchi, H., He, M., Wu, P., Kim, S., Paik, R., Sugino, K., Kvitsiani, D., Fu, Y., Lu, J., Lin, Y., et al. (2011). A resource of Cre driver lines for genetic targeting of GABAergic neurons in cerebral cortex. Neuron *71*, 995–1013.

Travers, J.B., Herman, K., and Travers, S.P. (2010). Suppression of third ventricular NPY-elicited feeding following medullary reticular formation infusions of muscimol. Behav. Neurosci. *124*, 225–233.

Travers, J.B., Yoo, J.E., Chandran, R., Herman, K., and Travers, S.P. (2005). Neurotransmitter phenotypes of intermediate zone reticular

formation projections to the motor trigeminal and hypoglossal nuclei in the rat. J. Comp. Neurol. *488*, 28–47.

Uematsu, M., Hirai, Y., Karube, F., Ebihara, S., Kato, M., Abe, K., Obata, K., Yoshida, S., Hirabayashi, M., Yanagawa, Y., and Kawaguchi, Y. (2008). Quantitative chemical composition of cortical GABAergic neurons revealed in transgenic venus-expressing rats. Cereb. Cortex *18*, 315–330.

Ushimura, A., Tsuji, T., Tanaka, S., Kogo, M., and Yamamoto, T. (2015). Neuropeptide-Y modulates eating patterns and masticatory muscle activity in rats. Behav. Brain Res. *278*, 520–526.

Walker, H.C., and Romsos, D.R. (1993). Similar effects of NPY on energy metabolism and on plasma insulin in adrenalectomized ob/ob and lean mice. Am. J. Physiol. *264*, E226–E230.

FIGURES

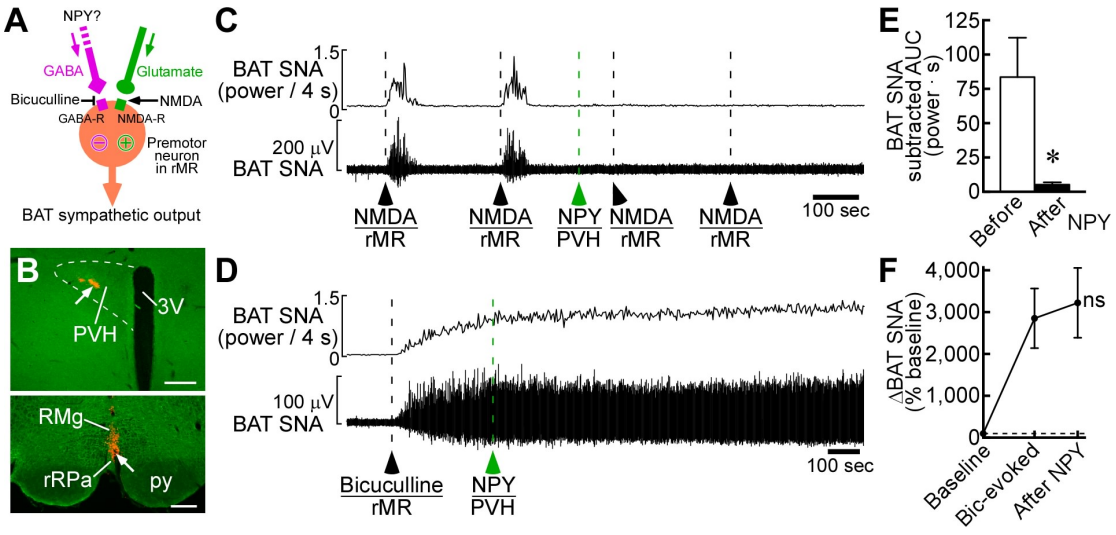

Figure 1. Hypothalamic NPY Inhibits BAT Thermogenesis through GABAergic Transmission to Sympathetic Premotor Neurons

(A) Sympathetic premotor neurons in the rMR are controlled by glutamatergic excitatory and GABAergic inhibitory inputs.

(B–D) NPY injection into the rat PVH suppressed increases in BAT SNA induced by NMDA nanoinjections into the rMR (C), but not that induced by blockade of $GABA_A$ receptors in the rMR with a bicuculline nanoinjection (D). Arrows in (B) show representative injection sites in the PVH (top) and rMR (bottom). Scale bars, 0.3 mm. 3V, third ventricle; py, pyramidal tract; RMg, raphe magnus nucleus; rRPa, rostral raphe pallidus nucleus.

(E) NMDA-induced changes in BAT SNA before and after NPY injection into the PVH (n = 5) are expressed as the area under the curve of the 'power/4 s' trace (C) above the pre-injection level (subtracted AUC) for 5 min after an NMDA injection. For data analysis, see Supplemental Experimental Procedures. $^*P < 0.05$ (unpaired t-test).

(F) Bicuculline-evoked (Bic-evoked) changes in BAT SNA and the effect of NPY injection into the PVH [from (D), n = 5]. ns: not significant (paired t-test *vs* Bic-evoked value). All values are means ± SEM. See also Figure S1 for all the injection sites and changes in other physiological variables.

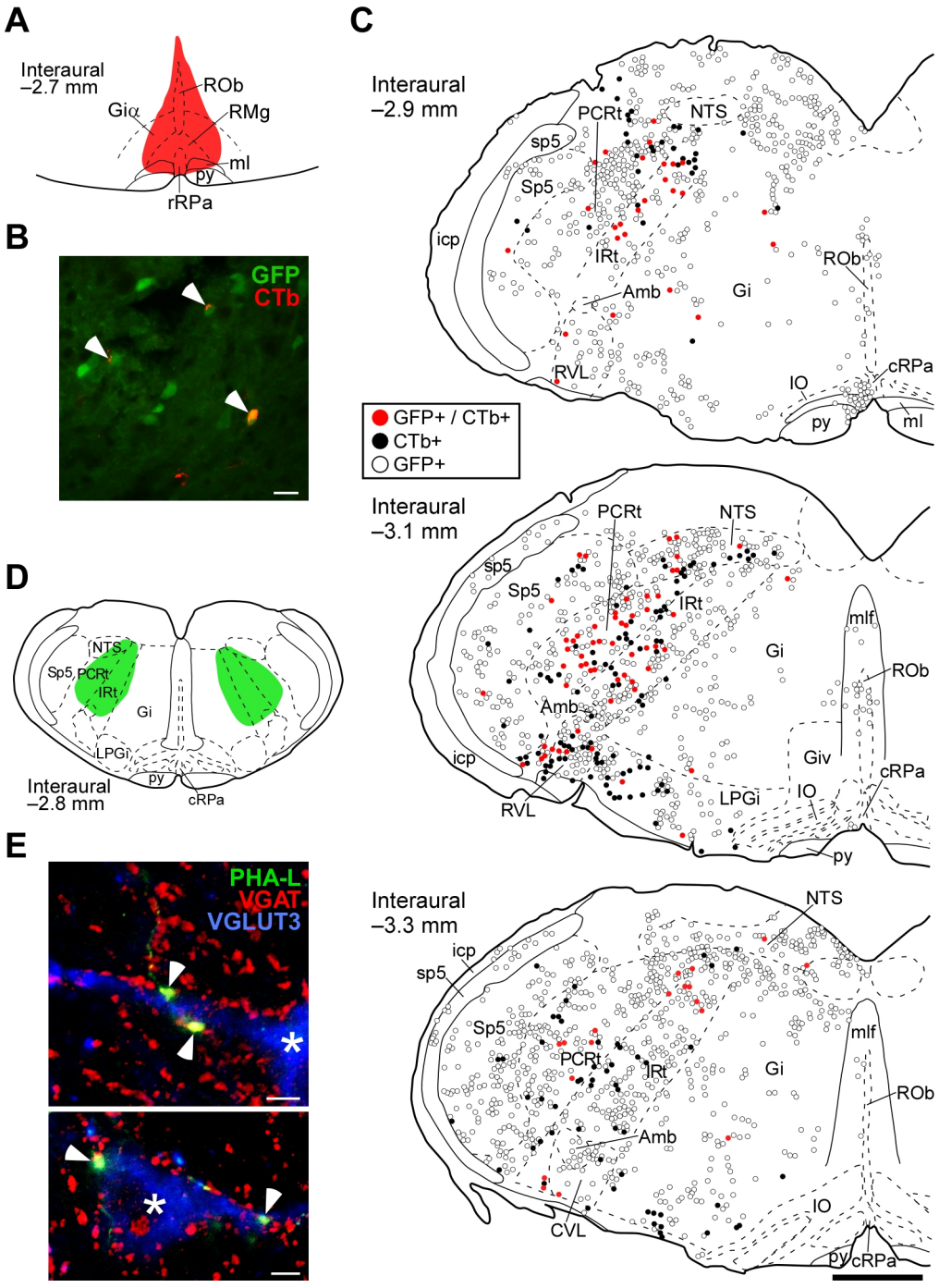

Figure 2. Putative Synaptic Inputs from GABAergic IRt/PCRt Neurons to Sympathetic Premotor Neurons in the rMR

(A–C) Retrograde tracing from the rMR in *Gad1-Gfp* knock-in mice. CTb injection into the rMR ([A], red) resulted in labeling of GFP-expressing neurons in the IRt/PCRt with CTb ([B], arrowheads). Drawings (C) show the distribution of CTb-labeled and GFP-expressing

neurons in the medulla oblongata (representative of 3 mice). Scale bars, 30 μm (B), 0.5 mm (C). Amb, ambiguus nucleus; cRPa, caudal raphe pallidus nucleus; Gi, gigantocellular reticular nucleus; Giα, alpha part of the gigantocellular reticular nucleus; Giv, ventral part of the gigantocellular reticular nucleus; icp, inferior cerebellar peduncle; IO, inferior olivary complex; LPGi, lateral paragigantocellular nucleus; ml, medial lemniscus; mlf, medial longitudinal fasciculus; ROb, raphe obscurus nucleus; sp5, spinal trigeminal tract; Sp5, spinal trigeminal nucleus.

(D and E) Anterograde tracing from the IRt/PCRt to the rMR in rats. PHA-L was injected bilaterally into the IRt/PCRt ([D], green). Arrowheads in the pseudocolored confocal images (E) indicate apposition of PHA-L-labeled, VGAT-containing axon swellings to dendrites and cell bodies of VGLUT3-immunoreactive neurons (asterisk, cell body) in the rMR (representative of 3 rats). Scale bar, 5 μm.

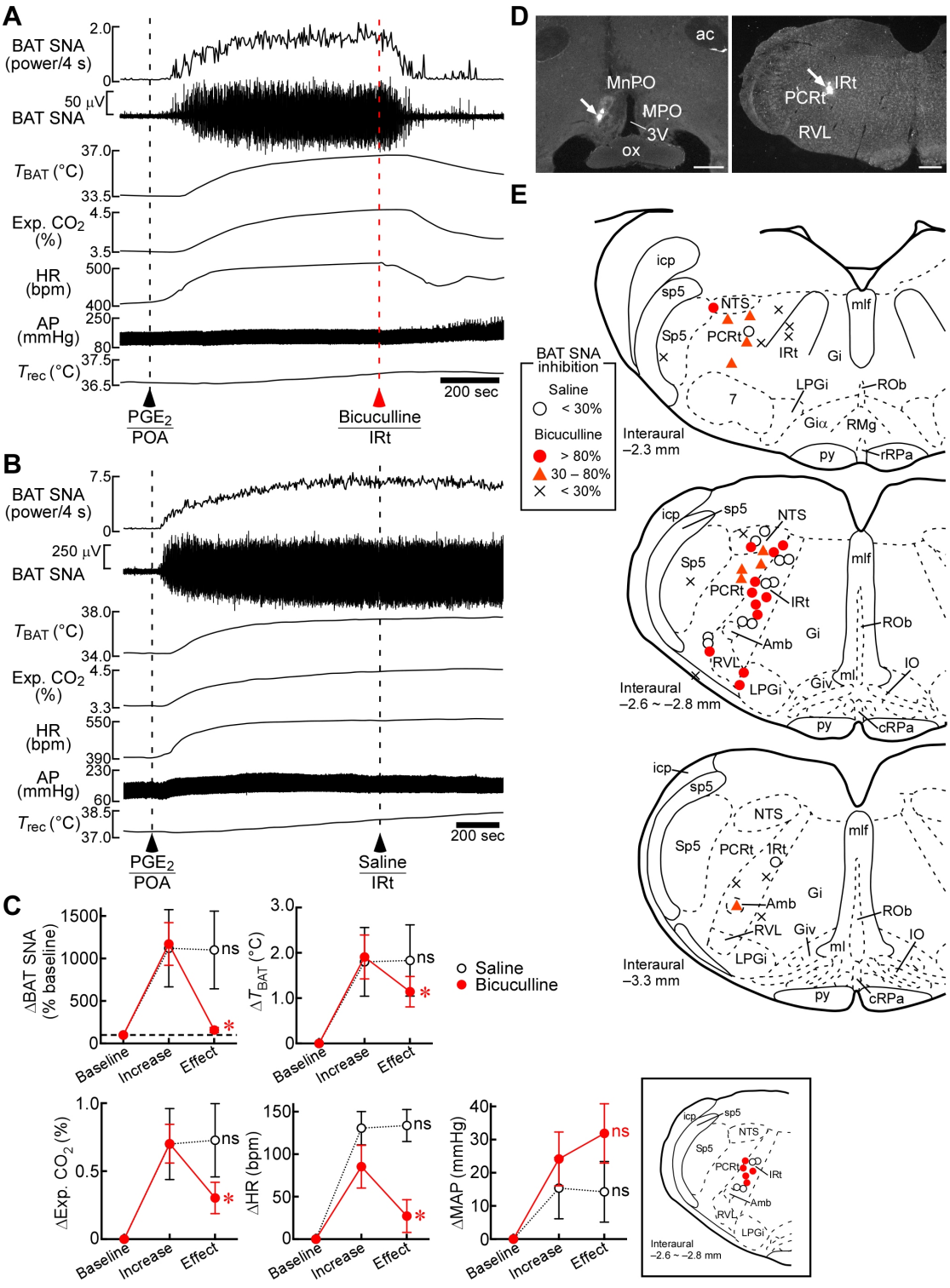

Figure 3. Stimulation of IRt/PCRt Neurons Reverses Febrile BAT Thermogenesis, Metabolism and Tachycardia

(A and B) Unilateral nanoinjection of bicuculline (A), but not saline (B), into the rat IRt reversed increases in BAT SNA, BAT temperature (T_{BAT}),

expired (Exp.) CO_2 and heart rate (HR) evoked by PGE_2 injection into the preoptic area (POA). AP, arterial pressure; T_{rec}, rectal temperature.

(C) PGE_2-evoked changes in physiological variables and the effect of bicuculline or saline injection into the IRt/PCRt at interaural –2.6 ~ –2.8 mm (n = 4 for saline, n = 5 for bicuculline). The boxed map shows the sites of injections chosen for these group data from (E). The PGE_2-evoked "Increase" values and the "Effect" values after the injection into the IRt/PCRt are shown. For data analysis, see Supplemental Experimental Procedures. ns: not significant, *$P < 0.05$ (paired t-test *vs* Increase values). All values are means ± SEM.

(D) Representative views of injection sites in the POA (left) and IRt (right). Scale bars, 0.5 mm. ac, anterior commissure; MnPO, median preoptic nucleus; MPO, medial preoptic area; ox, optic chiasm.

(E) Composite drawings that map sites of saline and bicuculline injections with their inhibitory effects on PGE_2-stimulated BAT SNA. 7, facial nucleus.

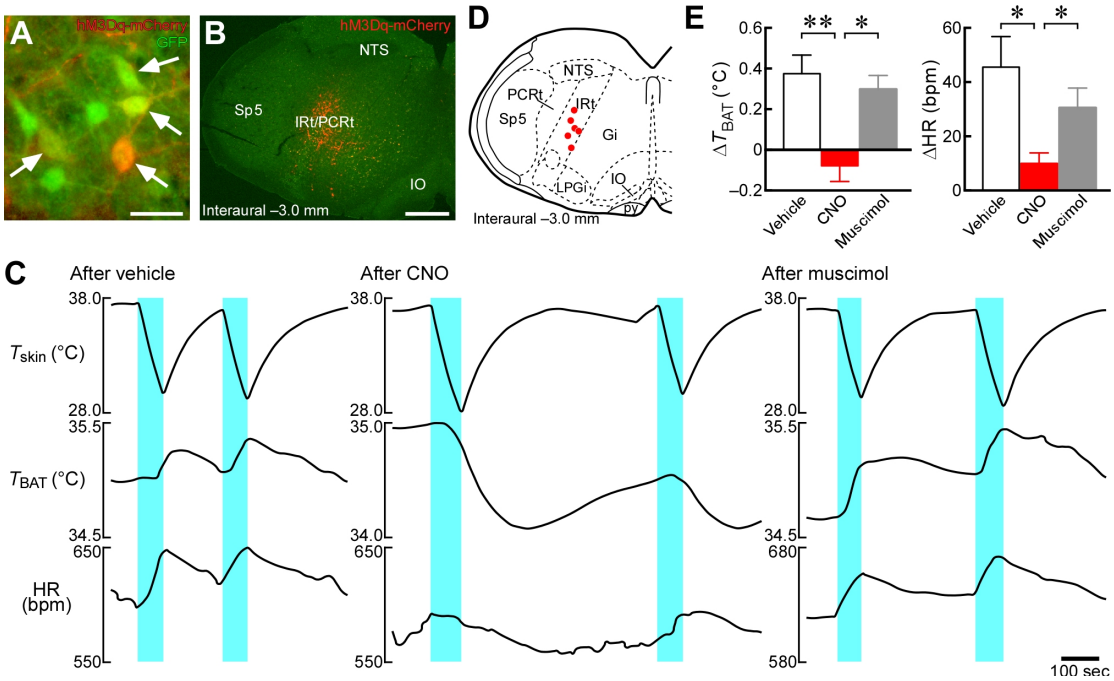

Figure 4. Chemogenetic Stimulation of GABAergic IRt/PCRt Neurons Eliminates Cooling-Induced BAT Thermogenesis and Tachycardia

(A) Selective expression of hM3Dq-mCherry (arrows) in GFP-expressing GABAergic neurons in the IRt/PCRt of a *Gad2-IRES-Cre*/*Gad1-Gfp* double knock-in mouse injected with AAV-EF1α-DIO-hM3Dq-mCherry into the IRt/PCRt. Scale bar, 30 μm.

(B) Distribution of hM3Dq-mCherry-expressing neurons in a *Gad2-IRES-Cre* knock-in mouse injected with AAV-EF1α-DIO-hM3Dq-mCherry into the IRt/PCRt. Scale bar, 0.5 mm.

(C) Effects of bilateral nanoinjections of vehicle, CNO and muscimol into the IRt/PCRt of a *Gad2-IRES-Cre* knock-in mouse injected with AAV-EF1α-DIO-hM3Dq-mCherry on BAT thermogenesis and tachycardia induced by trunk skin cooling (blue periods).

(D) Sites of drug injections. Vehicle, CNO and muscimol were injected at the same sites. The left side of the symmetric bilateral injection sites is shown.

(E) Cooling-induced changes in T_{BAT} and HR ($n = 6$). For data analysis, see Supplemental Experimental Procedures. $*P < 0.05$, $**P < 0.01$ (Tukey's multiple comparisons test following repeated measures one-way ANOVA). All values are means ± SEM.

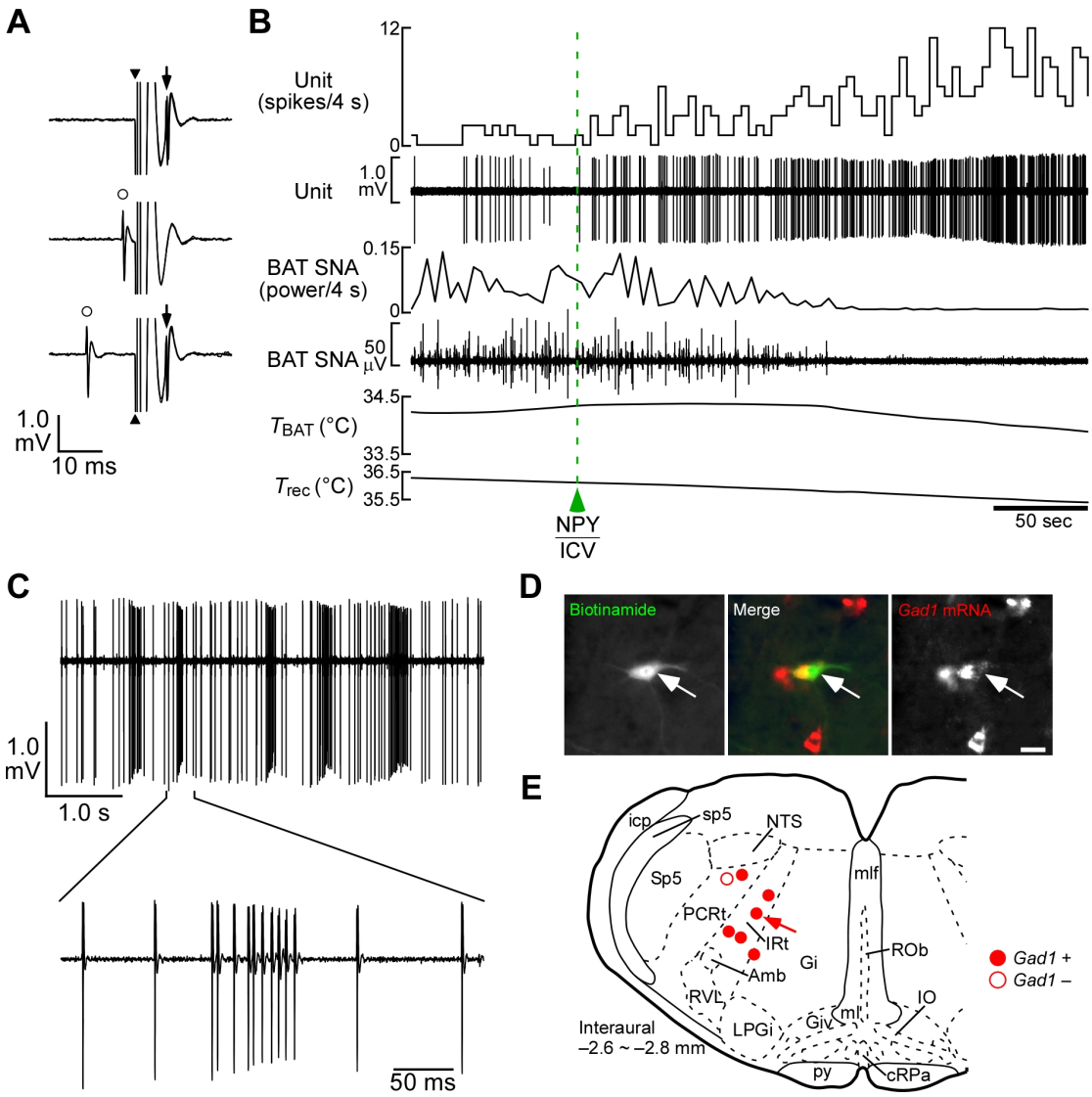

Figure 5. NPY-Mediated Neural Signaling Activates GABAergic IRt/PCRt Neurons Innervating the rMR

(A–C) *In vivo* extracellular unit recording of action potentials of a rat IRt/PCRt neuron. A collision test (A) shows an axonal projection of the IRt/PCRt neuron to the rMR. Single pulse stimulation in the rMR (triangles) evoked a constant-onset latency (6.7 ms) response in this neuron (arrow, top trace). rMR stimulation at 2.0 ms after a spontaneous action potential (open circle) failed to evoke a response of this neuron (middle trace). rMR stimulation at 10.0 ms after a spontaneous action potential evoked a constant-onset latency response of

this neuron (bottom trace). All traces are superpositions of 3 stimulation trials. An intracerebroventricular (ICV) NPY injection ([B], arrowhead) increased the firing rate of this neuron (unit) and reversed BAT SNA and T_{BAT} that had been increased by moderate body cooling. Obvious phasic bursting (C) was exhibited by some antidromically identified IRt/PCRt neurons following an ICV NPY injection.

(D) Histochemical identification of a recorded IRt/PCRt neuron innervating the rMR with juxtacellular labeling (green, arrow). *In situ* hybridization revealed that this neuron expressed *Gad1* (GAD67) mRNA (red). Scale bar, 30 μm.

(E) Location of rMR-projecting IRt/PCRt neurons successfully identified with juxtacellular labeling. Among them, all neurons activated by NPY injection expressed *Gad1* (filled circles), whereas the *Gad1*-negative one did not respond to NPY injection (open circle). Arrow indicates the neuron shown in (D).

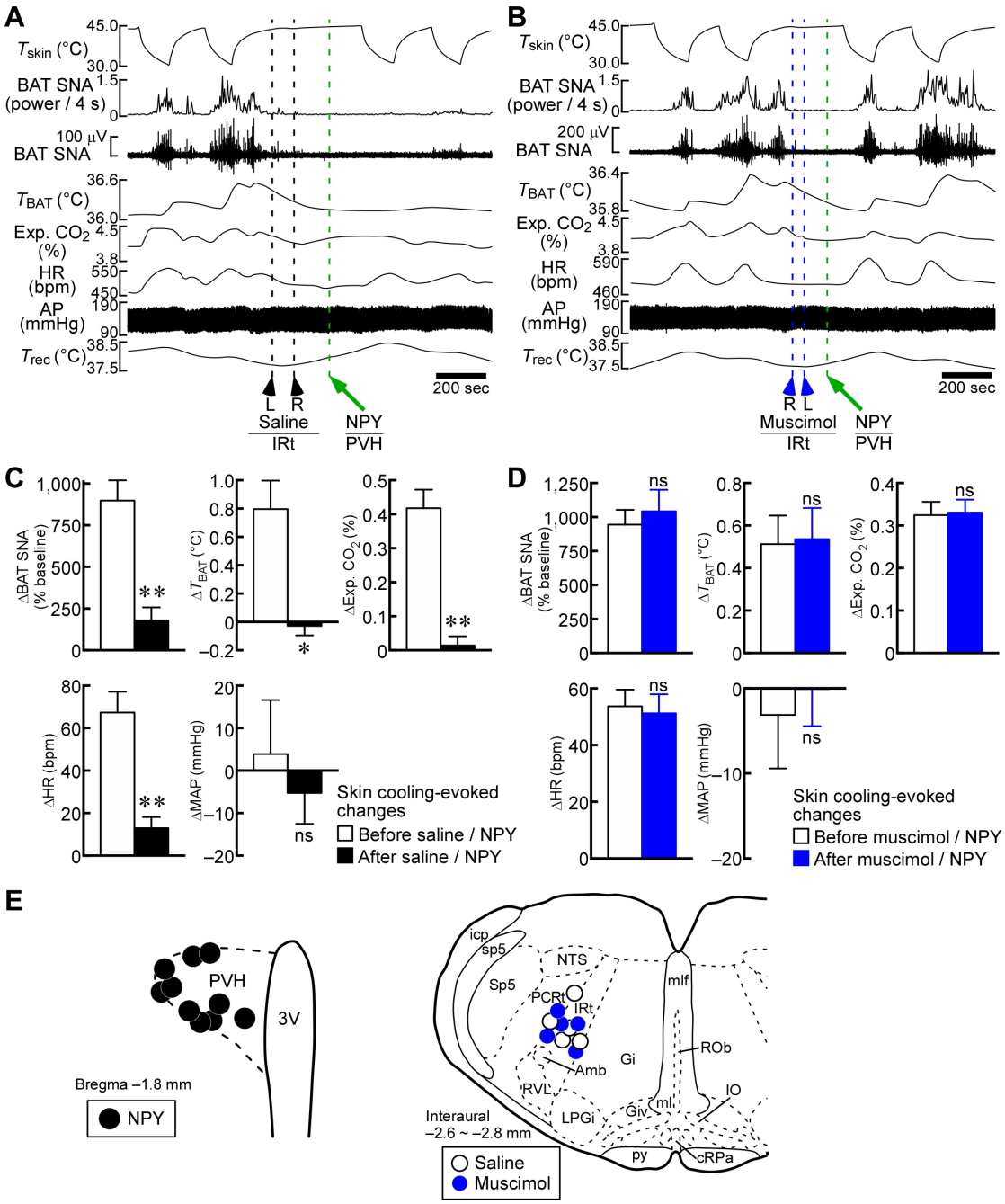

Figure 6. Hypothalamic NPY-Induced Inhibition of BAT Thermogenesis, Metabolism and Tachycardia Requires Activation of IRt/PCRt Neurons

(A and B) Skin cooling (T_{skin})-evoked increases in BAT thermogenesis, metabolism and HR were inhibited by NPY nanoinjection into the rat PVH following bilateral nanoinjections of saline into the IRt/PCRt (A),

whereas bilateral nanoinjections of muscimol into the IRt/PCRt prevented the NPY-evoked inhibition (B).

(C and D) Effects of bilateral saline (C) and muscimol (D) nanoinjections into the IRt/PCRt on NPY-induced inhibition of skin cooling-evoked BAT thermogenic, metabolic and tachycardic responses. Skin cooling-evoked changes in physiological variables before and after saline or muscimol injections into the IRt/PCRt and NPY injection into the PVH are compared ($n = 5$). For data analysis, see Supplemental Experimental Procedures. ns: not significant, $*P < 0.05$, $**P < 0.01$ (paired t-test). All values are means ± SEM.

(E) Sites of injections into the PVH (left) and IRt/PCRt (right). For the IRt/PCRt, the left side of the symmetric bilateral injection sites is shown.

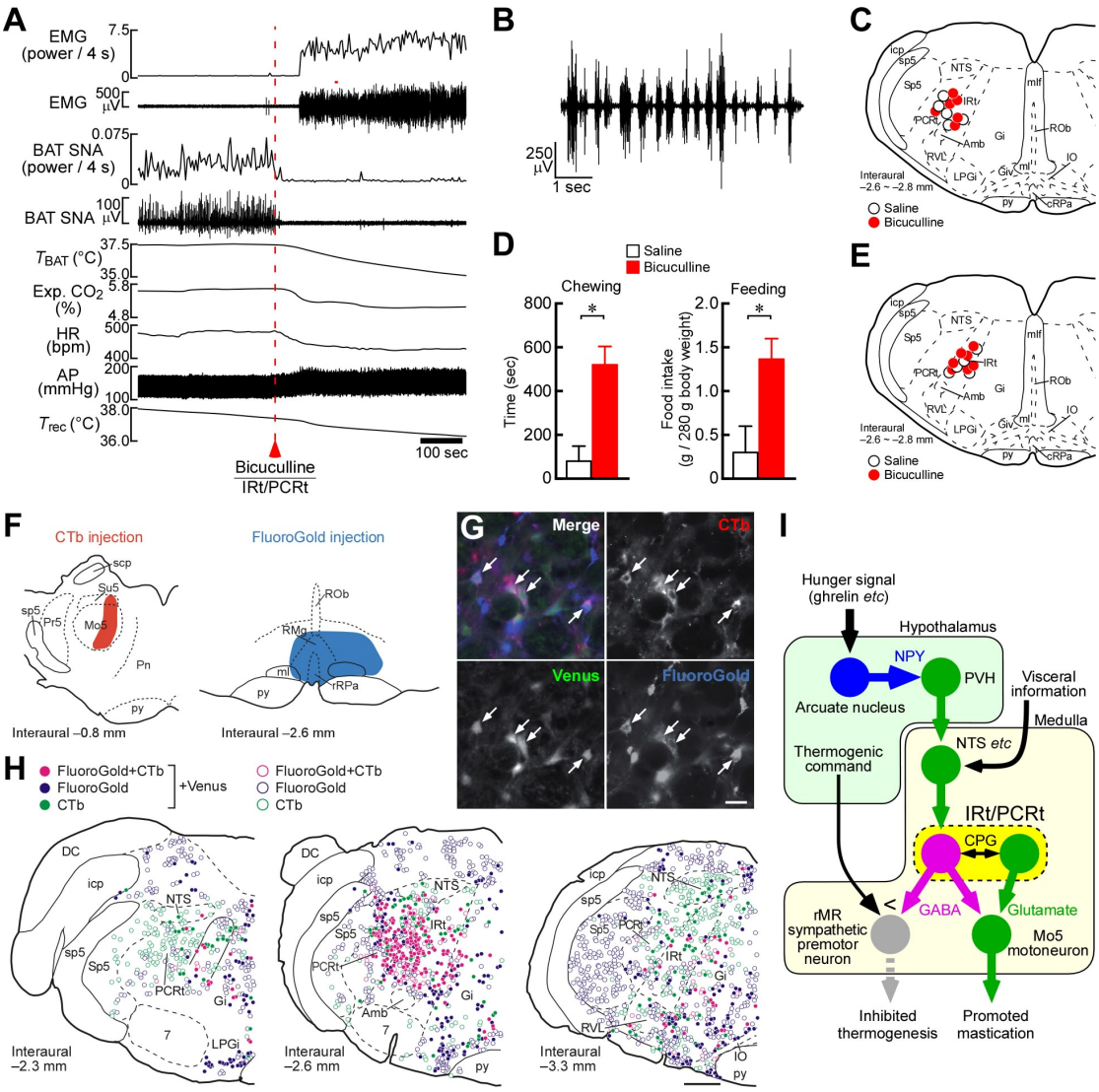

Figure 7. Stimulation of IRt/PCRt Neurons Promotes Mastication and Feeding As Well As Inhibits BAT Thermogenesis

(A–C) Unilateral nanoinjection of bicuculline into the IRt/PCRt in anesthetized rats (C) elicited mastication and inhibited cooling-evoked BAT thermogenesis and tachycardia (A). The masseter electromyogram (EMG) chart ([A], red horizontal bar) is expanded in (B). Figure S5B shows group data.

(D and E) Bicuculline injection into the IRt/PCRt in free-moving rats (E) increased chewing time and food intake measured for 1 hr after the

injection (D) (saline: $n = 5$, bicuculline, $n = 7$). $^{*}P < 0.05$ (Mann-Whitney test). All values are means ± SEM.

(F–H) Double retrograde labeling of GABAergic IRt/PCRt neurons with CTb injected into the Mo5 and with FluoroGold injected into the rMR (F) in an *Slc32a1-Venus* transgenic rat. Venus-expressing IRt/PCRt neurons were labeled with both CTb and FluoroGold ([G], arrows). Drawings (H) show the medullary distribution of CTb-labeled neurons and FluoroGold-labeled neurons with or without expression of Venus. Scale bars, 30 μm (G), 0.5 mm (H). DC, dorsal cochlear nucleus; Pn, pontine nuclei; Pr5, principal sensory trigeminal nucleus; scp, superior cerebellar peduncle; Su5, supratrigeminal nucleus.

(I) A model of the circuit that drives hunger responses. NPY-mediated signaling from the hypothalamus activates GABAergic IRt/PCRt neurons (red) to inhibit BAT thermogenesis. These GABAergic neurons facilitate rhythmic excitation of masticatory motoneurons potentially by interacting with glutamatergic neurons constituting the central pattern generator (CPG).

Supplemental Information for

Medullary Reticular Neurons Mediate Neuropeptide Y-Induced Metabolic Inhibition and Mastication

Yoshiko Nakamura, Yuchio Yanagawa, Shaun F. Morrison, and Kazuhiro Nakamura

Published in *Cell Metabolism* 25: 322–334, 2017
http://dx.doi.org/10.1016/j.cmet.2016.12.002

Inventory of Supplemental Information

1. Supplemental Figures

Supplemental Figure S1

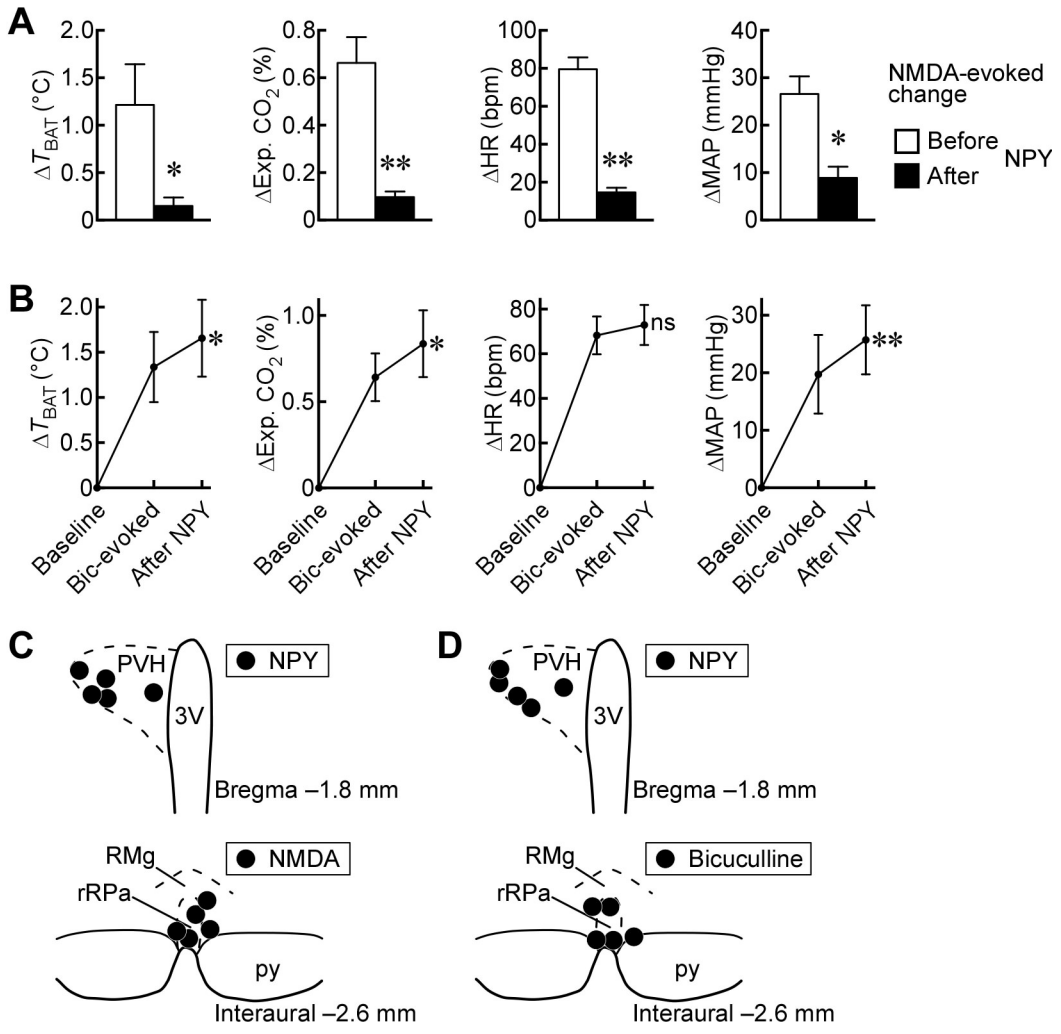

Figure S1. Hypothalamic NPY Inhibits BAT Thermogenesis and Cardiovascular Responses through GABAergic Transmission to Sympathetic Premotor Neurons, Related to Figure 1

(A) Changes in BAT temperature (T_{BAT}), expired (Exp.) CO_2, HR and mean arterial pressure (MAP) that were induced by NMDA nanoinjection into the rMR before and after NPY injection into the PVH (n = 5). The NMDA-evoked changes in these variables are the differences between their baseline values and their peak values within 5 min after an NMDA injection. For data analysis, see Supplemental

Experimental Procedures. *$P < 0.05$, **$P < 0.01$ (paired *t*-test). All values are means ± SEM.

(B) Changes in T_{BAT}, Exp. CO_2, HR and MAP that were induced by bicuculline nanoinjection into the rMR and those following the subsequent nanoinjection of NPY into the PVH ($n = 5$). The graphed values are the bicuculline-evoked (Bic-evoked) increases in all the physiological variables and the values after the NPY injection. For data analysis, see Supplemental Experimental Procedures. ns: not significant, *$P < 0.05$, **$P < 0.01$ (paired *t*-test *vs* Bic-evoked values). All values are means ± SEM.

(C and D) Sites of NPY injections in the PVH (top) and NMDA and bicuculline injections in the rMR (bottom).

Supplemental Figure S2

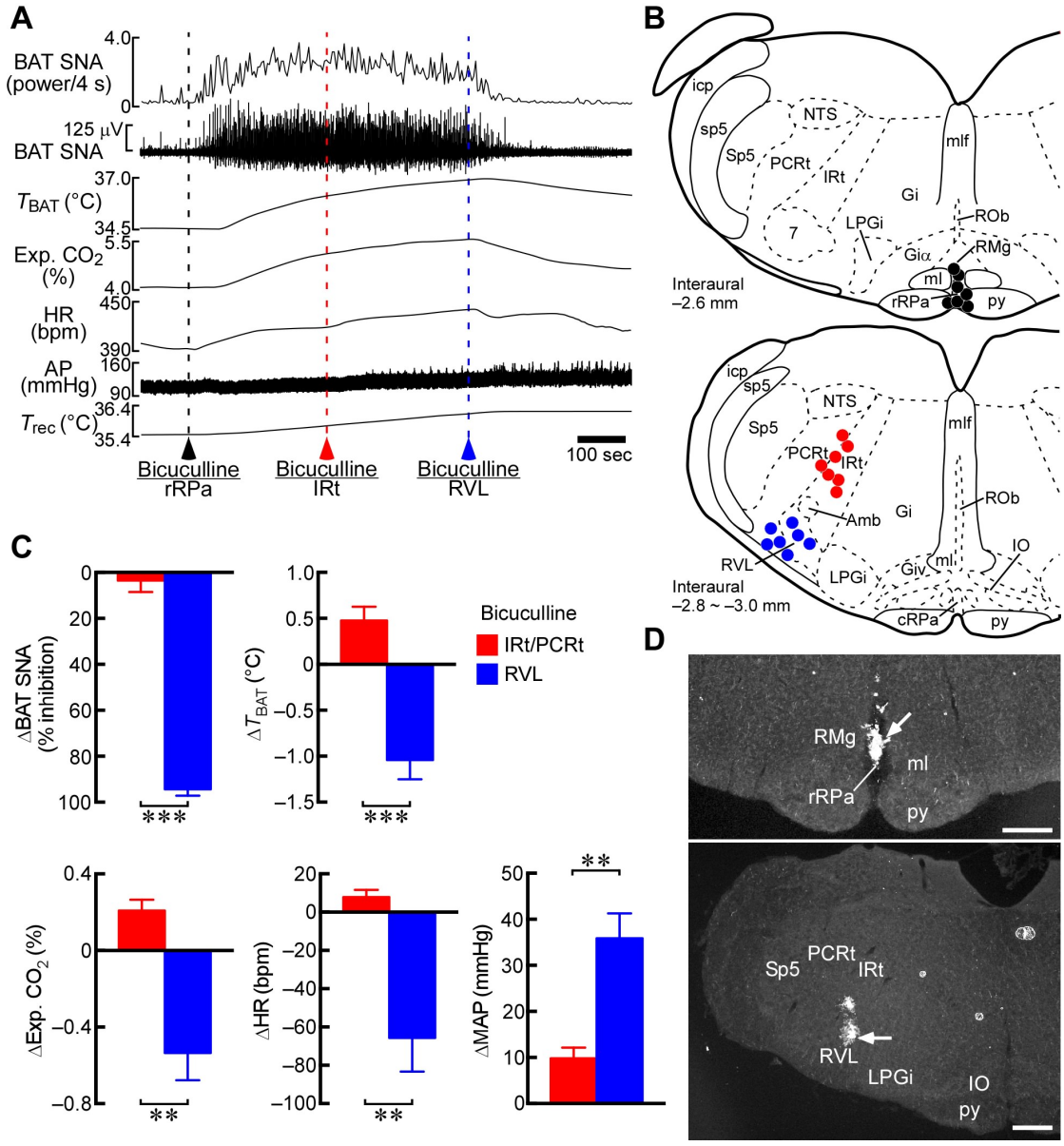

Figure S2. Stimulation of IRt/PCRt Neurons and RVL Neurons Exerts Different Effects on BAT Thermogenic, Metabolic and Tachycardic Responses Evoked by Antagonizing $GABA_A$ Receptors in the rMR, Related to Figure 3

(A) BAT thermogenic, metabolic and tachycardic responses evoked by a bicuculline nanoinjection into the rat rMR were not inhibited by a unilateral nanoinjection of bicuculline into the IRt, but were reversed by a unilateral nanoinjection of bicuculline into the RVL.

(B) Sites of bicuculline injections into the rMR (black circles), IRt/PCRt (red) and RVL (blue).

(C) Changes in the physiological variables following bicuculline injection into the IRt/PCRt and subsequent bicuculline injection into the RVL (n = 7). Differences between the pre-injection values (averages during the 1-min period immediately before bicuculline injection into the IRt/PCRt or RVL) and post-injection values (averages during the 1-min period beginning at 2 min after the injection) are shown. $^{**}P < 0.01$, $^{***}P < 0.001$ (paired t-test). All values are means ± SEM.

(D) Representative views of injection sites (arrows) in the rMR (top) and RVL (bottom). Scale bars, 0.5 mm.

Supplemental Figure S3

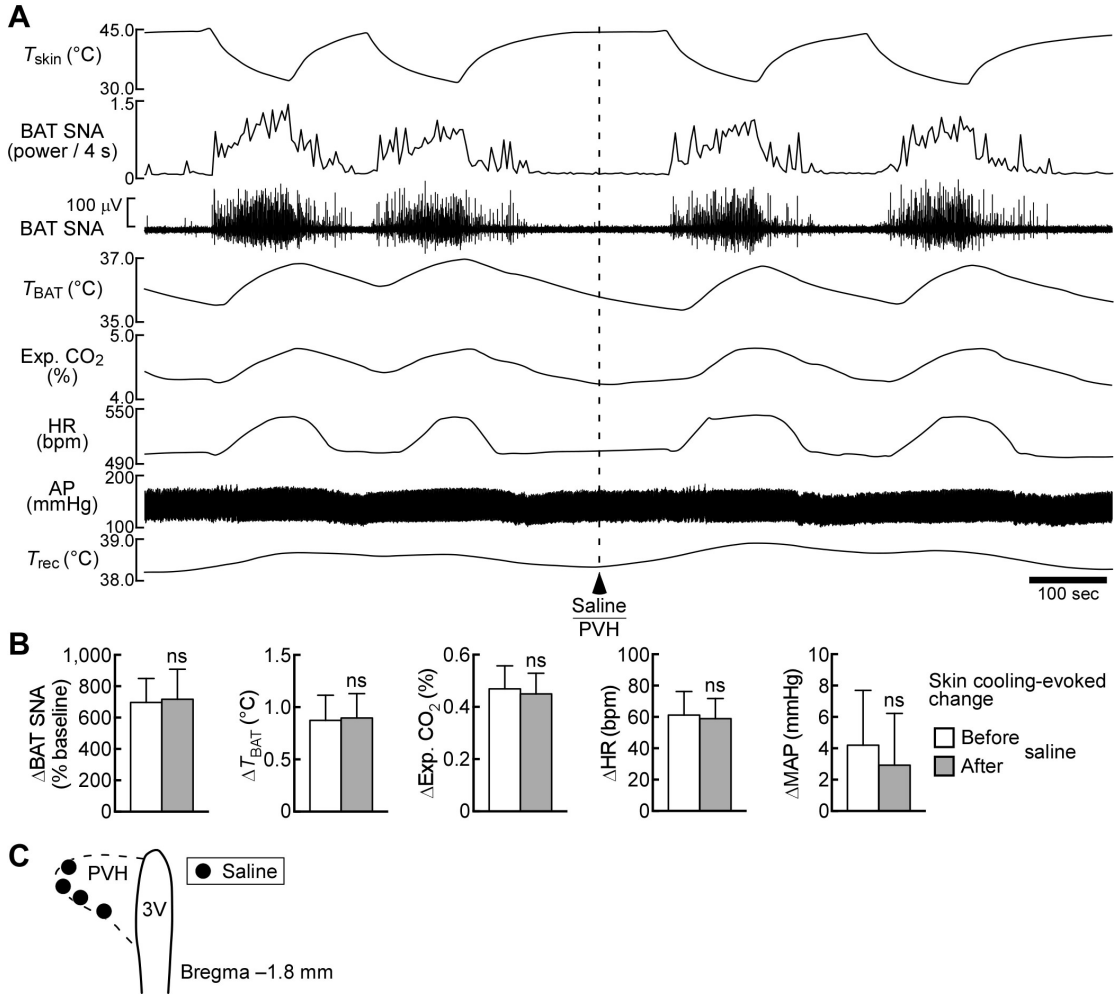

Figure S3. Saline Injection into the PVH Has No Effect on Skin Cooling-Evoked BAT Thermogenic, Metabolic and Tachycardic Responses, Related to Figure 6

(A) Trunk skin cooling-evoked increases in BAT SNA, T_{BAT}, Exp. CO_2 and HR were not affected by a saline nanoinjection into the PVH.

(B) Skin cooling-evoked changes in physiological variables before and after saline injection into the PVH (n = 4). For data analysis, see Supplemental Experimental Procedures. ns: not significant (paired t-test). All values are means ± SEM.

(C) Sites of saline injections into the PVH.

Supplemental Figure S4

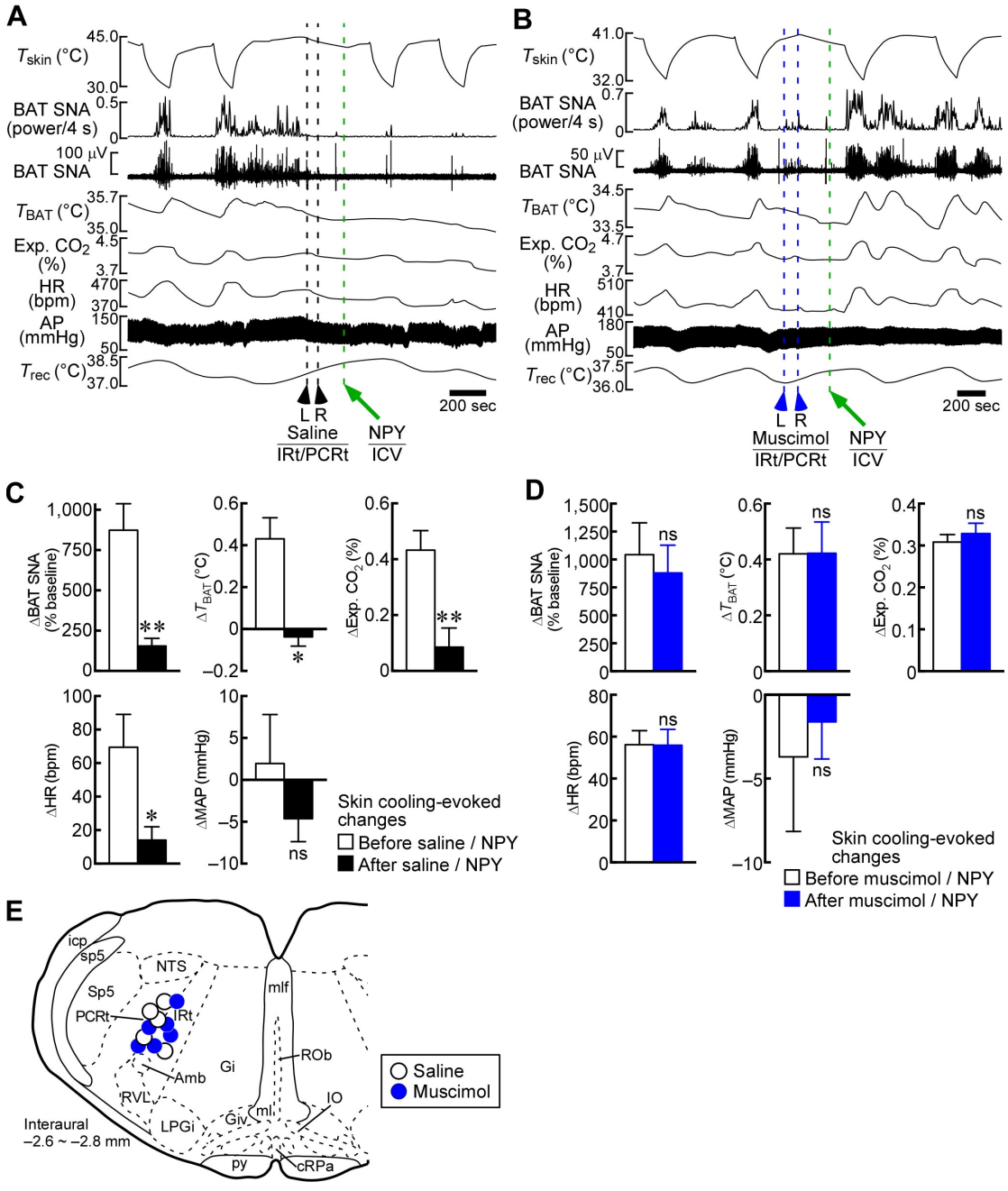

Figure S4. Inactivation of IRt/PCRt Neurons Eliminates Inhibitory Effects of Intracerebroventricular (ICV) NPY Injection on Skin Cooling-Evoked BAT Thermogenic, Metabolic and Tachycardic Responses, Related to Figure 6

(A and B) Skin cooling-evoked increases in BAT thermogenesis, metabolism and HR were inhibited by NPY injection into the rat lateral ventricle following bilateral nanoinjections of saline into the IRt/PCRt (A), but not following those of muscimol (B).

(C and D) Effects of bilateral saline (C) and muscimol (D) injections into the IRt/PCRt on NPY-induced inhibition of skin cooling-evoked BAT thermogenic, metabolic and tachycardic responses. Skin cooling-evoked changes in physiological variables before and after saline or muscimol injections into the IRt/PCRt and ICV NPY injection are compared (n = 5 for saline, n = 6 for muscimol). For data analysis, see Supplemental Experimental Procedures. ns: not significant, *P < 0.05, **P < 0.01 (paired t-test). All values are means ± SEM.

(E) Sites of injections into the IRt/PCRt. The left side of the symmetric bilateral injection sites is shown.

Supplemental Figure S5

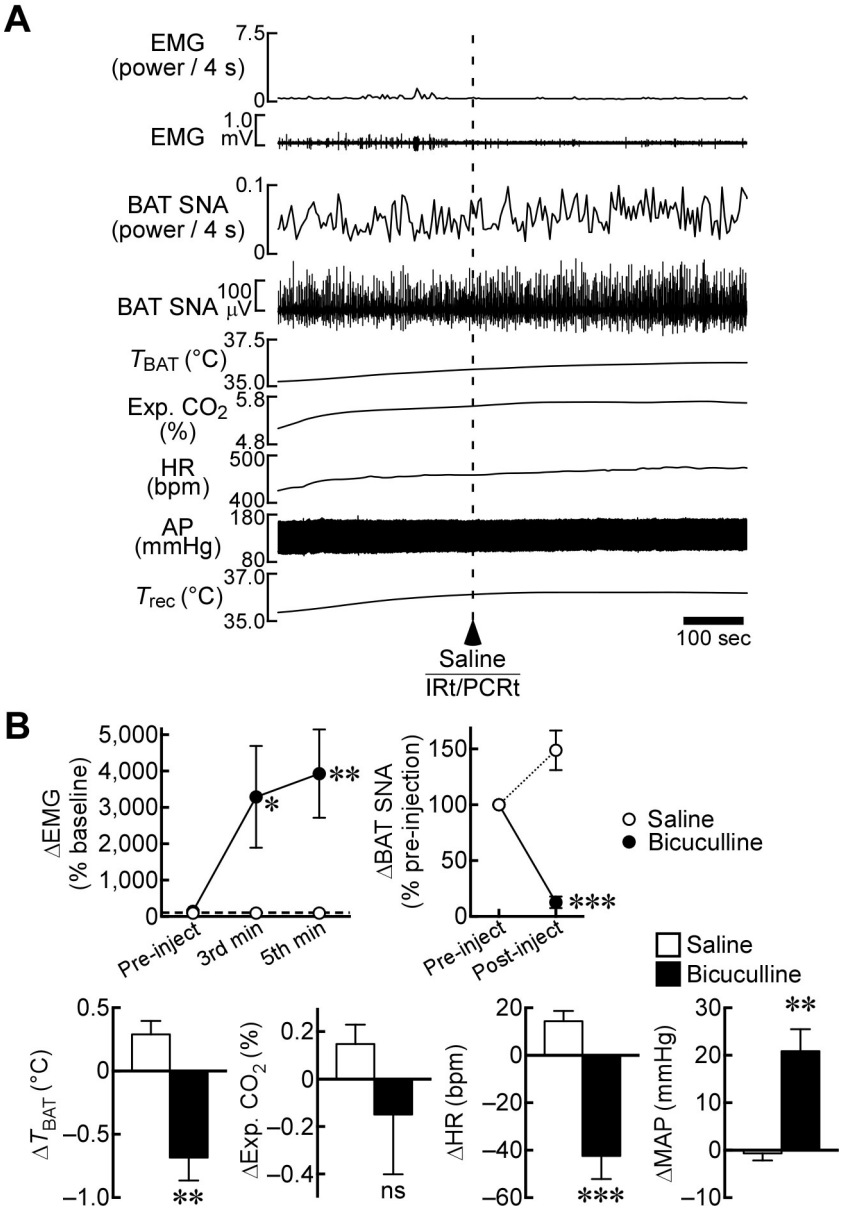

Figure S5. **Stimulation of IRt/PCRt Neurons Elicits Mastication As Well As Inhibits BAT Thermogenesis and Tachycardia, Related to Figure 7A–C**

(A) A saline nanoinjection into the rat IRt/PCRt had no effect on masseter EMG or cooling-evoked elevation of BAT SNA, T_{BAT}, Exp. CO_2 or HR. Compare with Figure 7A.

(B) Changes in physiological variables that were evoked by saline (n = 5) or bicuculline (n = 6) nanoinjection into the IRt/PCRt. Differences between pre-injection baseline values (Pre-inject) and post-injection values (Post-inject) are shown.

The effect on EMG was evaluated with the averages during the 1-min period beginning at 2 min after the injection (3rd min) and during the 1-min period beginning at 4 min after the injection (5th min). For data analysis, see Supplemental Experimental Procedures. Injection sites are shown in Figure 7C. ns: not significant, $*P < 0.05$, $**P < 0.01$, $***P < 0.001$ (unpaired *t*-test *vs* Saline for BAT SNA, T_{BAT}, Exp. CO_2, HR and MAP; Bonferroni's multiple comparison test following a two-way ANOVA *vs* Saline for EMG). All values are means ± SEM.

Supplemental Figure S6

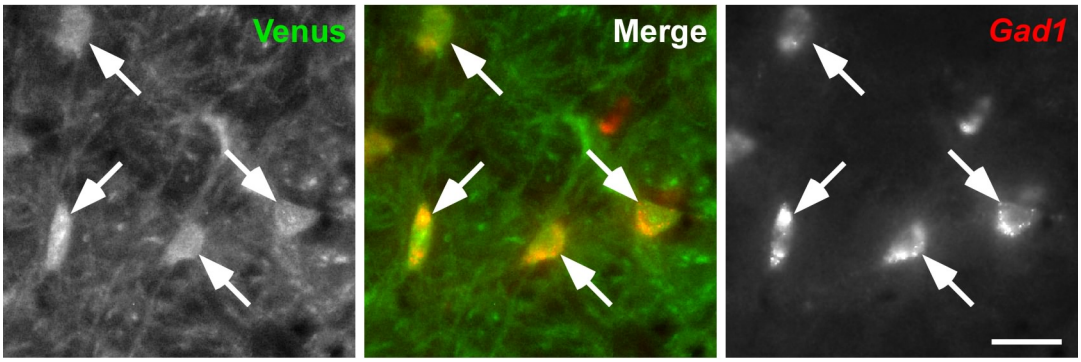

Cell counting in IRt/PCRt (interaural –2.3 ~ –3.3 mm)

$$\frac{\text{Double positive cells}}{\text{Venus+ cells}} = 94\% \ (1803 / 1909)$$

$$\frac{\text{Double positive cells}}{\textit{Gad1}\text{+ cells}} = 95\% \ (1803 / 1902)$$

Figure S6. Selectivity of Venus Expression in GABAergic Neurons in the IRt/PCRt in *Slc32a1-Venus* Transgenic Rats, Related to Figure 7F–H

Medullary sections of an *Slc32a1-Venus* transgenic rat were subjected to immunohistochemistry for Venus and *in situ* hybridization for *Gad1* (GAD67) mRNA, a marker for GABAergic neurons. Arrows indicate cells expressing both Venus and *Gad1*. Venus-expressing cells and *Gad1*-expressing cells in the IRt/PCRt (interaural –2.3 ~ –3.3 mm) were counted in every sixth 30-μm-thick frontal section. Scale bar, 30 μm.

Supplemental Figure S7

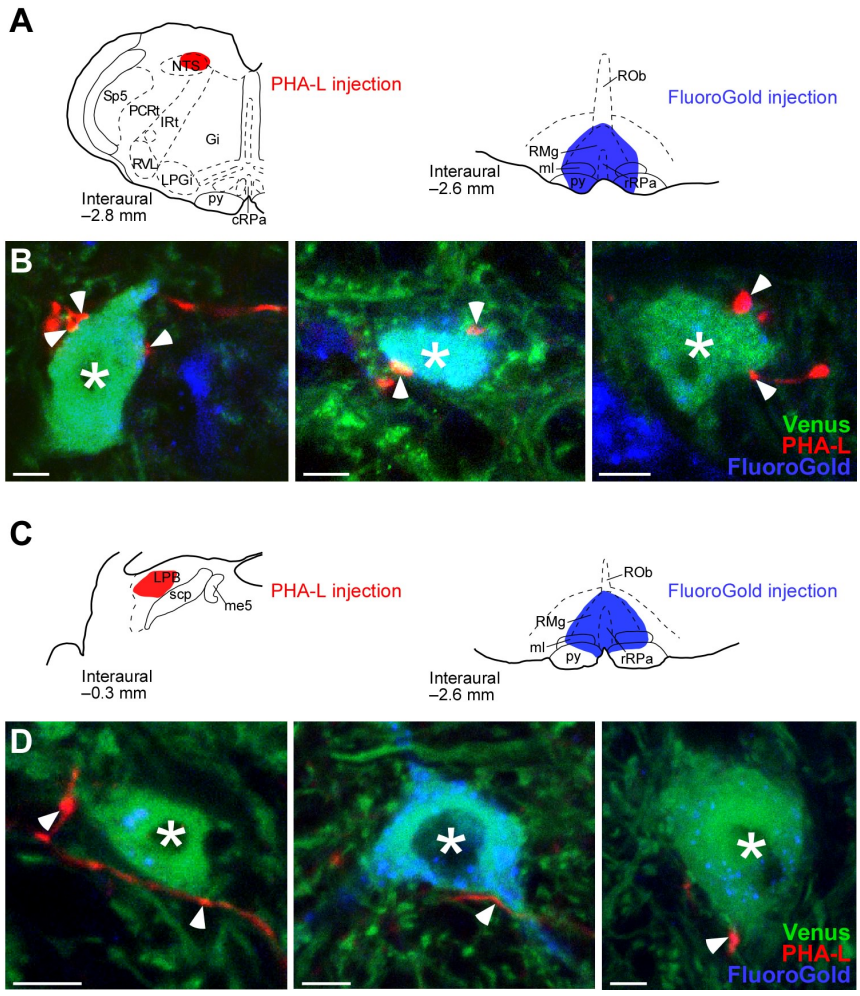

Figure S7. GABAergic IRt/PCRt Neurons Projecting to the rMR Receive Putative Synaptic Connections from the Rostral NTS and LPB, Related to Figure 7I

(A and B) PHA-L and FluoroGold were injected into the rostral NTS and the rMR of an *Slc32a1-Venus* transgenic rat, respectively (A). Arrowheads in the pseudocolored confocal images (B) indicate apposition of PHA-L-labeled axon swellings to FluoroGold-labeled, Venus-expressing cell bodies (asterisks) in the IRt/PCRt. Three examples of confocal images are shown. Scale bars, 5 μm.

(C and D) PHA-L and FluoroGold were injected into the LPB and the rMR of an *Slc32a1-Venus* transgenic rat, respectively (C). Arrowheads in the pseudocolored confocal images (D) indicate apposition of PHA-L-labeled axon swellings to FluoroGold-labeled, Venus-expressing cell bodies (asterisks) in the IRt/PCRt. Three

examples of confocal images are shown. Scale bars, 5 μm. me5, mesencephalic trigeminal tract.

2. Supplemental Movies

Movie S1. Mastication elicited by bicuculline nanoinjection into the rat IRt/PCRt, Related to Figure 7A–C

Bicuculline was nanoinjected into the IRt/PCRt under urethane-chloralose anesthesia. Needle electrodes were inserted into the masseter muscle for EMG recording.

Available at

http://dx.doi.org/10.1016/j.cmet.2016.12.002

3. Supplemental Experimental Procedures

Tracer injection

Animals were deeply anesthetized with chloral hydrate (280 mg/kg, i.p.) following gas anesthesia with 3% isoflurane in 100% O_2. They were then placed in a stereotaxic apparatus and the incisor bar level was adjusted so that the bregma and lambda were at the same dorsal level. For retrograde tracing, 1 μg/μl Alexa594-conjugated CTb (Invitrogen) and/or 4% FluoroGold (Fluorochrome) was pressure-injected at the rMR (rat: 2.6 mm posterior to the interaural line, on the midline, 9.5–9.7 mm ventral to the brain surface; mouse: 2.6–2.7 mm posterior to the interaural line, on the midline, 4.7 mm ventral to the brain surface) and/or at the Mo5 (rat: 0.5–0.8 mm posterior to the interaural line, 2.0 mm lateral to the midline, 6.5 mm ventral to the brain surface) through a glass micropipette (tip inner diameter 10–20 μm) with the aid of a Picospritzer II (General Valve). For anterograde tracing, a 2.5% solution of PHA-L (Vector), dissolved in 10 mM sodium phosphate buffer (pH 8.0), was iontophoretically injected into the IRt/PCRt (rat: 2.6–2.8 mm posterior to the interaural line, 1.8–2.0 mm lateral to the midline, 7.0 mm ventral to the brain surface) through a glass micropipette by applying a +2.0 μA constant current with 7-sec on–off cycles for 20–30 min per site, or into the NTS (rat: 2.8 mm posterior to the interaural line, 1.7 mm lateral to the midline, 6.0 mm ventral to the brain surface) or LPB (rat: 0.3 mm posterior to the interaural line, 2.0–2.2 mm lateral to the midline, 5.2 mm ventral to the brain surface) by applying the same current for 30 min.

Immunohistochemistry

Immunohistochemical procedures were based on our previous studies (Nakamura et al., 2004, 2005). For double immunofluorescence staining of CTb and GFP or Venus, brain sections were incubated overnight with a mixture of an anti-CTb goat serum (1:10,000) and an anti-GFP mouse antibody (1 μg/ml). The anti-GFP antibody showed cross-reactivity to Venus. After a rinse, the sections were incubated for 1 hr with 10 μg/ml Alexa594-conjugated donkey antibody to goat IgG

(A11058, Invitrogen). After blocking with 10% normal goat serum for 30 min, the sections were incubated for 1 hr with 10 μg/ml Alexa488-conjugated goat antibody to mouse IgG (A11029, Invitrogen) in the presence of 10% normal goat serum.

For double immunofluorescence staining of PHA-L and Venus, sections were incubated overnight with a mixture of an anti-PHA-L rabbit antibody (1 μg/ml) and an anti-GFP mouse antibody (1 μg/ml). After a rinse, the sections were incubated for 1 hr with a mixture of a biotinylated donkey antibody to rabbit IgG (1:100; AP182B, Millipore) and 10 μg/ml Alexa488-conjugated goat antibody to mouse IgG. The sections were then incubated for 1 hr with 2 μg/ml Alexa594-conjugated streptavidin (S11227, Invitrogen).

For double immunofluorescence staining of GFP and mCherry, sections were incubated overnight with a mixture of an anti-GFP guinea pig serum (1:500) and an anti-mRFP rabbit antibody (0.5 μg/ml). The anti-mRFP antibody showed cross-reactivity to mCherry. After a rinse, the sections were incubated for 1 hr with a mixture of 10 μg/ml Alexa488-conjugated goat antibody to guinea pig IgG (A11073, Invitrogen) and 10 μg/ml Alexa594-conjugated goat antibody to rabbit IgG (A11037, Invitrogen).

For triple immunofluorescence staining for PHA-L, VGLUT3 and VGAT, sections were incubated overnight with a mixture of an anti-PHA-L goat antibody (1 μg/ml), an anti-VGLUT3 guinea pig antibody (0.5 μg/ml) and an anti-VGAT rabbit antibody (1:1,000). After a rinse, the sections were incubated for 1 hr with 10 μg/ml Alexa546-conjugated donkey antibody to goat IgG (A11056, Invitrogen). After blocking with 10% normal goat serum for 30 min, the sections were incubated for 1 hr with 10 μg/ml Alexa647-conjugated goat antibody to rabbit IgG (A21245, Invitrogen) and a horseradish peroxidase-conjugated donkey antibody to guinea pig IgG (1:100; AP193P, Millipore) in the presence of 10% normal goat serum. The sections were then incubated with fluorescein-conjugated tyramide (Tyramide Signal Amplification fluorescence systems; 1:50; PerkinElmer) for 1 min.

The stained sections were thoroughly washed and mounted onto glass slides. Following coverslipped, they were observed under an epifluorescence microscope (Eclipse 80i, Nikon) or under a confocal laser-scanning microscope (LSM 5 PASCAL or LSM880-ELYRA PS.1, Zeiss, or TCS SP8, Leica).

In vivo physiological recordings in anesthetized rats

Surgery and data acquisition. The procedure for *in vivo* electrophysiology basically followed our previous studies (Nakamura and Morrison, 2007, 2011). SD rats were anesthetized intravenously with urethane (0.8 g/kg) and α-chloralose (80 mg/kg) after cannulation of a femoral artery, a femoral vein, and the trachea under anesthesia with 3% isoflurane in 100% O_2. They were then placed in a stereotaxic apparatus and the incisor bar level was adjusted so that the bregma and lambda were at the same dorsal level. To record arterial pressure and heart rate (HR), the arterial cannula was attached to a pressure transducer. The trunk was shaved, a copper-constantan thermocouple to monitor skin temperature was taped onto the abdominal skin, and the trunk was wrapped with a plastic water jacket to cool and re-warm the skin. The rats were positioned in a stereotaxic apparatus with a spinal clamp, paralysed with D-tubocurarine (0.6 mg i.v. initial dose, supplemented with 0.3 mg/hr), and artificially ventilated with 100% O_2 (60 cycles/min, tidal volume: 3.5 ml) to stabilize BAT nerve recording by preventing respiration-related movements as well as cooling-induced shivering. Mixed expired CO_2 (Exp. CO_2) was measured using a capnometer to provide an index of changes in whole body metabolism and was maintained at 3.5–4.5% under basal conditions. Rectal temperature was monitored as an indication of core body temperature using a thermocouple inserted into the rectum and was maintained at 37.0–37.5˚C by perfusing the water jacket with cold and warm water.

Postganglionic BAT SNA was recorded from the central cut end of a nerve bundle isolated from the ventral surface of the right interscapular BAT pad after dividing it along the midline and reflecting it laterally. The nerve bundle was placed

on bipolar hook electrodes and soaked in mineral oil. Nerve activity was filtered (1–300 Hz) and amplified (× 5,000–50,000) with a CyberAmp 380 (Axon Instruments). BAT temperature (T_{BAT}) was monitored with a thermocouple inserted into the intact left interscapular BAT pad. Animals for EMG recording, which had no injection with D-tubocurarine, were instrumented with bipolar needle electrodes inserted into the masseter muscle. The EMG signal was filtered (10–1,000 Hz) and amplified (× 2,000) with CyberAmp 380. The physiological variables were digitized and recorded onto a personal computer using Spike2 software (CED).

Drug injections. Nanoinjections of drugs into the brain were made with the aid of a Picospritzer II through a glass micropipette (20–30 μm tip inner diameter) perpendicularly inserted into the brain. All the drugs were dissolved into pyrogen-free 0.9% saline (Otsuka). In experiments to examine the effect of NPY injection into the PVH on thermogenic, metabolic and cardiovascular responses to rMR stimulation (Figures 1 and S1), rats received nanoinjections of NMDA (0.2 mM, 60 nl; Sigma) or bicuculline (2 mM, 60 nl; Sigma) into the rMR combined with a unilateral nanoinjection of NPY (1 mg/ml, 60 nl; Bachem, H-6375) into the PVH (1.8 mm posterior to bregma, 0.6 mm lateral to the midline, 7.7 mm ventral to the brain surface). In experiments to examine the effect of IRt/PCRt stimulation on febrile thermogenic, metabolic and cardiovascular responses (Figure 3), animals received a unilateral nanoinjection of PGE_2 (1 mg/ml, 60 nl; Sigma) into the preoptic area (0.1–0.2 mm anterior to bregma, 0.5 mm lateral to the midline, 8.0–8.5 mm ventral to the brain surface). Approximately 10 min after the PGE_2 injection, bicuculline (2 mM) or saline was unilaterally nanoinjected (60 nl) into a medullary area including the IRt/PCRt, NTS and RVL. In experiments to compare the effects of IRt/PCRt and RVL stimulation on physiological responses induced by disinhibition of rMR neurons (Figure S2), bicuculline (2 mM, 60 nl) was first nanoinjected into the rMR. Approximately 5 min after the bicuculline injection, bicuculline (2 mM, 60 nl) was unilaterally nanoinjected into the IRt/PCRt. Another 5 min after the bicuculline injection into the IRt/PCRt, bicuculline (2 mM, 60 nl) was unilaterally nanoinjected

into the RVL (2.8–3.0 mm posterior to the interaural line, 2.0–2.5 mm lateral to the midline, 7.5–8.0 mm ventral to the brain surface).

In experiments involving trunk skin cooling (Figures 6, S3 and S4), animals received repeated cooling episodes: each cooling lasted for 150–200 s until the skin temperature was lowered to a level consistent with preceding cooling episodes and then the skin was re-warmed by switching to perfusion of the water jacket with warm water. After control cooling episodes, muscimol (2 mM) or saline was bilaterally nanoinjected (100 nl each) into the IRt/PCRt, followed by a unilateral nanoinjection of NPY (1 mg/ml, 60 nl) into the PVH or by an NPY injection into the lateral ventricle (1 mg/ml, 5 μl; 0.8 mm posterior to bregma, 1.4 mm lateral to the midline and 4.0 mm ventral to the skull surface) using a Hamilton syringe. The animals subsequently received repeated cooling episodes. In experiments recording masseter EMG (Figures 7A–C and S5), bicuculline (2 mM) or saline was unilaterally nanoinjected (60 nl) into the IRt/PCRt during active BAT thermogenesis evoked by moderate cooling, which never evoked shivering.

To mark the injection sites, 0.2% fluorescent microspheres (0.1 μm diameter; FluoSpheres, F8801 or F8803; Invitrogen) in saline was nanoinjected at the same stereotaxic coordinates through the same micropipette. In some experiments, the drug solutions injected contained 0.01% fluorescent microspheres. After the physiological recordings, the animals were transcardially perfused with a 4% formaldehyde solution and the brain was removed and cryoprotected in a 30% sucrose solution overnight. After the tissue was sectioned at a thickness of 40 μm with a freezing microtome, the locations of the injections were identified by detecting the fluorescent microspheres under an epifluorescence microscope.

Data analysis. BAT SNA and EMG amplitudes were quantified (Spike2) in sequential 4 s bins as the square root of the total power (root mean square) in the 0–20 Hz (BAT SNA) and 0–500 Hz (EMG) band of the autospectra of each 4 s segment of the traces. The "power/4 s" traces were used for quantification and statistical analyses of changes in BAT SNA and EMG.

In experiments to examine the effect of NPY injection into the PVH on physiological responses evoked by NMDA injections into the rMR (Figures 1C and E and S1A), baseline (pre-injection) values of BAT SNA, T_{BAT}, Exp. CO_2, HR and mean arterial pressure (MAP) were obtained from the averages during the 1-min period immediately prior to NMDA injection. The NMDA-evoked changes in T_{BAT}, Exp. CO_2, HR and MAP were the differences between their baseline values and their peak values within 5 min after NMDA injection. The NMDA-evoked changes in BAT SNA were the area under the curve (AUC) of the 'power/4 s' trace (Figure 1C) above the baseline level (subtracted AUC) for 5 min after NMDA injection. In experiments to examine the effect of NPY injection into the PVH on physiological responses evoked by bicuculline injections into the rMR (Figures 1D and F and S1B), baseline values of BAT SNA, T_{BAT}, Exp. CO_2, HR and MAP were obtained from the averages during the 1-min period immediately prior to bicuculline injection. The values of the bicuculline-evoked increases in all the physiological variables were obtained from the averages during the 1-min period immediately before NPY injection into the PVH. The values following NPY injection were obtained from the averages during the 1-min period beginning at 2 min after the NPY injection.

In experiments to examine the effect of IRt/PCRt stimulation on febrile thermogenic, metabolic and cardiovascular responses (Figure 3A–C), baseline values of BAT SNA, T_{BAT}, Exp. CO_2, HR and MAP were the averages during the 1-min period immediately prior to PGE_2 injection. The PGE_2-evoked "Increase" values of these variables were the averages during the 1-min period immediately before bicuculline or saline injection into the IRt. The "Effect" values of these variables after the injection into the IRt were the averages during the 1-min period beginning at 2 min after the injection.

In experiments to compare the effects of IRt/PCRt and RVL stimulation on physiological responses evoked by disinhibition of rMR neurons (Figure S2), pre-injection values of BAT SNA, T_{BAT}, Exp. CO_2, HR and MAP were obtained from the averages during the 1-min period immediately before bicuculline injection into the

IRt/PCRt or RVL. Post-injection values of these variables were obtained from the averages during the 1-min period beginning at 2 min after the bicuculline injection.

In experiments involving trunk skin cooling (Figures 6, S3 and S4), baseline (pre-cooling) values of BAT SNA, T_{BAT}, Exp. CO_2, HR and MAP were the averages during the 30-sec period immediately prior to the initiation of each skin cooling. Skin cooling-evoked response values for T_{BAT}, Exp. CO_2 and HR were obtained at the end of skin cooling (at switching to re-warming), and those for BAT SNA and MAP were obtained from the averages during the 30-sec period immediately prior to the end of skin cooling.

In experiments involving masseter EMG recording (Figures 7A and S5), pre-injection baseline values of EMG, BAT SNA, T_{BAT}, Exp. CO_2, HR and MAP were obtained from the averages during the 1-min period immediately prior to bicuculline or saline injection into the IRt/PCRt. Post-injection values for T_{BAT}, Exp. CO_2 and HR after the injection into the IRt/PCRt were obtained at 3 min after the injection, and those for MAP and BAT SNA were obtained from the averages during the 1-min period beginning at 2 min after the injection. The effect of the injection on EMG was evaluated with the averages during the 1-min period beginning at 2 min after the injection (3rd min) and during the 1-min period beginning at 4 min after the injection (5th min).

AAV Production

The AAV expressing the Cre-dependent *hM3Dq-mCherry* transgene (AAV2/1-EF1α-DIO-hM3Dq-mCherry) was created with pAAV-EF1α-DIO-hM3Dq-mCherry (donated by Bryan Roth: addgene#50460) and purified by following the modified Gene Transfer Targeting and Therapeutics Core protocol at Salk Institute (http://vectorcore.salk.edu/protocols.php). Required plasmids were transfected into HEK293T cells and AAV was purified from a crude lysate of the cells by ultracentrifugation using OptiPrep (Axis-Shield, Oslo, Norway). Following

concentration using a membrane filter (Amicon Ultra-15 NMWL 50K, Millipore), the final titration was 1.34 x 10^{11} IFU.

***In vivo* recordings of BAT thermogenesis and heart rate in anesthetized mice**

Gad2-IRES-Cre knock-in mice that received bilateral injections into the IRt/PCRt with AAV-EF1α-DIO-hM3Dq-mCherry more than 1 week before were anesthetized with urethane (1.3 g/kg, i.p.). They were then placed in a stereotaxic apparatus and the incisor bar level was adjusted so that the bregma and lambda were at the same dorsal level. To monitor skin temperature, the trunk was shaved and a copper-constantan thermocouple was taped onto the abdominal skin. The trunk was placed on a plastic water jacket and the abdominal skin was cooled by perfusing the water jacket with ice-cold water and then rewarmed by switching to perfusion with warm water. Rectal temperature was monitored using a thermocouple inserted into the rectum and maintained by perfusing the water jacket with warm or cold water. T_{BAT} was monitored with a needle-type thermocouple inserted into the interscapular BAT pad. To monitor HR, electrocardiogram (ECG) was recorded using needle electrodes inserted into the skin. The ECG signal was filtered (1–1,000 Hz), amplified (× 2,000–5,000) with CyberAmp 380, digitized, and recorded onto a personal computer using Spike2 software (CED) to calculate heart rate.

To analyze skin cooling-induced changes in T_{BAT} and HR (Figure 4E), baseline values of T_{BAT} and HR were obtained from the averages during the 30-sec period immediately prior to skin cooling. Skin cooling-induced response values for HR were obtained at the end of the skin cooling and those for T_{BAT} were obtained at 30 sec after the end of the skin cooling. Skin cooling-evoked changes in these variables from their baseline values were compared among skin cooling episodes after vehicle, CNO and muscimol injections into the IRt/PCRt.

Bicuculline injection into the IRt/PCRt in free-moving rats

SD rats were deeply anesthetized with chloral hydrate (280 mg/kg, i.p.) following gas anesthesia with 3% isoflurane in 100% O_2. They were positioned in a stereotaxic apparatus and a sterile stainless guide cannula (ID = 0.29 mm, OD = 0.56 mm; C316G; Plastic One) was inserted to target the IRt/PCRt at a backward leaning angle of 12° to avoid penetration through the vestibular nucleus. The inserted guide cannula was anchored with dental cement to stainless steel screws attached to the skull. A dummy cannula cut to the exact length of the guide cannulae was inserted into the guide cannula to avoid clogging. An internal cannula for injection (see below) with the thickness to fit the guide cannulae was cut to be long enough to allow the injector tip to protrude 2.3 mm below the tip of the guide cannula. All the incisions in the skin were closed with suture and the wounds were treated with iodine. The rats were given an injection of an ampicillin sodium solution (0.2 ml, 125 mg/ml) into femoral muscles to avoid infection and recovered from the surgery under regular health check with individual housing in feeding monitoring cages (Feedam, Melquest). During the recovery period, the animals were habituated to the experimenters and injection procedures once every day. Animals displaying obvious signs of sickness, such as anorexia and severe weight loss, during the recovery period were excluded.

One week after the surgery, the internal cannula was connected to Teflon tubing and filled with 1 mM bicuculline or pyrogen-free saline. A 10-µl Hamilton syringe filled with mineral oil was connected to the other end of the Teflon tubing. The dummy cannula that had been inserted into the guide cannula was gently removed and the internal cannula was inserted into the guide cannula. Then, the bicuculline or saline solution was slowly ejected (50–100 nl) through the cannula using a manually operated syringe manipulator (Narishige). The injection volume was visually confirmed by the movement of the aqua–oil interface along the Teflon tubing, which had been graduated. Food intake and chewing time were measured for 1 hr after the injection. Some animals injected with bicuculline chewed pieces of shredded bedding paper as well as food pellets, and hence, both behaviors were taken into the measurement of chewing time. At the end of the experiment, the rats received

another injection at the same site with 50 nl of fluorescent microspheres to label the site, which was then identified in the brain slices as described above.

4. Supplemental References

Nakamura, K., Matsumura, K., Hübschle, T., Nakamura, Y., Hioki, H., Fujiyama, F., Boldogköi, Z., König, M., Thiel, H.J., Gerstberger, R., et al. (2004). Identification of sympathetic premotor neurons in medullary raphe regions mediating fever and other thermoregulatory functions. J. Neurosci. *24*, 5370–5380.

Nakamura, K., and Morrison, S.F. (2007). Central efferent pathways mediating skin cooling-evoked sympathetic thermogenesis in brown adipose tissue. Am. J. Physiol. Regul. Integr. Comp. Physiol. *292*, R127–R136.

Nakamura, K., and Morrison, S.F. (2011). Central efferent pathways for cold-defensive and febrile shivering. J. Physiol. *589*, 3641–3658.

Nakamura, Y., Nakamura, K., Matsumura, K., Kobayashi, S., Kaneko, T., and Morrison, S.F. (2005). Direct pyrogenic input from prostaglandin EP3 receptor-expressing preoptic neurons to the dorsomedial hypothalamus. Eur. J. Neurosci. *22*, 3137–3146.